The GET pathway serves to activate Atg32-mediated mitophagy by ER targeting of the Ppg1-Far complex

Mashun Onishi[1] and Koji Okamoto[1]*

[1]Laboratory of Mitochondrial Dynamics, Graduate School of Frontier Biosciences, Osaka University, Suita, Osaka 565-0871, Japan

*Corresponding author.

E-mail address: kokamoto@fbs.osaka-u.ac.jp

Keywords: GET pathway; Atg32; Ppg1; Msp1; mitochondria; mitophagy

Condensed title: The GET pathway acts in promoting mitophagy

Abstract

Mitophagy removes defective or superfluous mitochondria via selective autophagy. In yeast, the pro-mitophagic protein Atg32 localizes to the mitochondrial surface and interacts with the scaffold protein Atg11 to promote degradation of mitochondria. Although Atg32-Atg11 interactions are thought to be stabilized by Atg32 phosphorylation, how this posttranslational modification is regulated remains obscure. Here we show that cells lacking the guided entry of tail-anchored proteins (GET) pathway exhibit reduced Atg32 phosphorylation and Atg32-Atg11 interactions, which can be rescued by additional loss of the ER-resident Ppg1-Far complex, a multi-subunit phosphatase negatively acting in mitophagy. In GET-deficient cells, Ppg1-Far is predominantly localized to mitochondria. An artificial ER anchoring of Ppg1-Far in GET-deficient cells significantly ameliorates defects in Atg32-Atg11 interactions and mitophagy. Moreover, disruption of GET and Msp1, an AAA-ATPase that extracts non-mitochondrial proteins localized to the mitochondrial surface, elicits synthetic defects in mitophagy. Collectively, we propose that the GET pathway mediates ER targeting of Ppg1-Far, thereby preventing dysregulated suppression of mitophagy activation.

Introduction

Mitochondria-specific autophagy, named mitophagy, is one of the membrane trafficking pathways conserved from yeast to humans. In this process, mitochondria are sequestrated by flattened double-membrane structures called isolation membranes and transported to the lysosome (in mammals) or the vacuole (in yeast), a lytic compartment, for degradation (Onishi and Okamoto, 2021; Onishi et al., 2021; Palikaras et al., 2018). In the budding yeast *Saccharomyces cerevisiae*, the outer mitochondrial membrane (OMM)-anchored protein Atg32 is phosphorylated in a manner dependent on casein kinase 2 (CK2) under mitophagy-inducing conditions (Aoki et al.,

2011; Kanki et al., 2013; Kanki et al., 2009; Kondo-Okamoto et al., 2012; Okamoto et al., 2009). This posttranslational modification increases the affinity of Atg32 for Atg11, a scaffold protein for assembly of core autophagy-related (Atg) proteins required for formation of autophagosomes encapsulating mitochondria (He et al., 2006; Mao et al., 2013). Conversely, Atg32 dephosphorylation is mediated by Ppg1, a PP2A-like phosphatase (Furukawa et al., 2018). Ppg1 interacts with the Far complex that acts in a cooperative manner to suppress Atg32 phosphorylation, Atg32-Atg11 interactions, and mitophagy (Furukawa et al., 2018). Together, the phosphorylation-dephosphorylation switch for Atg32 is likely to be a key regulatory step to initiate selective degradation of mitochondria.

Appropriate targeting of membrane proteins to correct subcellular destinations is critical to maintain functional compartments within cells (Barlowe and Miller, 2013). Tail-anchored (TA) proteins, which harbor a single transmembrane (TM) domain at the very C-terminus, are post-translationally inserted into the membranes of mitochondria, peroxisomes, and ER, acting in a myriad of cellular processes such as vesicular trafficking, protein import, and organelle dynamics (Barlowe and Miller, 2013). In budding yeast, multiple TA proteins are targeted to the ER via the guided entry of TA proteins (GET) pathway (Denic, 2012; Denic et al., 2013; Farkas and Bohnsack, 2021). Prior to insertion into the ER membrane, the TM domains of TA proteins are shielded by the cytosolic ATPase Get3 (Bozkurt et al., 2009; Mateja et al., 2015; Mateja et al., 2009; Suloway et al., 2009; Yamagata et al., 2010). Then, the Get3-TA protein complexes are recruited to the ER membrane-embedded Get1/2 insertase complex (McDowell et al., 2020; Schuldiner et al., 2008; Stefer et al., 2011; Wang et al., 2014; Wang et al., 2011). Successful interactions between Get1/2 and Get3 drive detachment of TA proteins from Get3, enabling their insertion into the ER membrane by the Get1/2 complex. Upon disruption of the GET pathway, several TA proteins are not properly localized to the ER, but instead, targeted to mitochondria

(Jonikas et al., 2009; Schuldiner et al., 2008). These ER-resident TA proteins on the OMM are removed by Msp1, a mitochondrial surface-anchored AAA-ATPase that extracts inappropriately targeted non-mitochondrial TA proteins and thus maintains mitochondrial membrane integrity (Chen et al., 2014; Okreglak and Walter, 2014; Wang et al., 2020; Wohlever et al., 2017; Zhang et al., 2011).

Our previous findings reveal a previously unappreciated role for Get1/2 in promoting mitophagy during prolonged respiratory growth (Onishi et al., 2018). In contrast to severely impaired mitophagy, other selective and bulk autophagy pathways are only slightly affected, indicating that the common core autophagy machinery itself is rarely altered in the absence of Get1/2 (Onishi et al., 2018). Although it is likely that the Get1/2 complex serves a specialized function in mitophagy, how this ER-resident TA protein insertase acts in degradation of mitochondria remains uncertain. In this study, we demonstrate that Atg32 phosphorylation and Atg32-Atg11 interactions are compromised in cells lacking Get components. Notably, perturbation of Ppg1-mediated Atg32 dephosphorylation mostly recovers Atg32-Atg11 interactions and mitophagy in *get1/2*-null cells. Moreover, the Ppg1-Far complex is localized to the ER in a manner dependent on the GET pathway, and loss of the Get components leads to targeting of this phosphatase complex to mitochondria. Artificial ER localization of the Far complex in the absence of Get1/2 significantly restores Atg32-Atg11 interactions and mitophagy. In addition, disruption of Msp1 extractase activity in GET-deficient cells causes an exacerbation in mitophagy defects. Taken together, our data suggest that the GET pathway serves to promote appropriate targeting of the Ppg1-Far complex to the ER, thereby contributing to Atg32 activation at the initial stage of mitophagy.

Results

Atg32 phosphorylation and Atg32-Atg11 interactions are reduced in cells lacking Get components

In yeast, mitophagy initiation consists of three main steps, expression, mitochondrial localization, and phosphorylation of Atg32. Based on our previous results that Get components are not critical for Atg32 expression and mitochondrial localization (Onishi et al., 2018), we sought to test if loss of Get components affects Atg32 phosphorylation in the early phase of mitophagy. Atg32 is phosphorylated when wild-type cells are grown in respiratory media containing non-fermentable carbon sources such as glycerol (Gly) (Kondo-Okamoto et al., 2012). Under these mitophagy-inducing conditions, putative phosphorylated Atg32 molecules appeared as multiple upper bands (Fig. 1 A) that were diminished by treatment with a protein phosphatase (Fig. 1 B). In contrast, these mobility shifts seemed to be reduced in *get1/get2/get3*-null cells, indicating that Get components are important for efficient phosphorylation of Atg32 (Fig. 1 A).

As Atg32 phosphorylation is thought to be a key regulatory step for stabilizing Atg32-Atg11 interactions (Aoki et al., 2011; Kondo-Okamoto et al., 2012), we next investigated whether loss of Get components impinges this protein-protein interaction for mitophagy. To address this issue, we applied the NanoBiT (NanoLuc Binary Technology, Promega) system, a luminescence-based assay for protein-protein interactions, to quantitative monitoring of Atg32-Atg11 interactions in live cells. When yeast cells expressing chromosomally integrated LgBiT-tagged Atg32 and SmBiT-tagged Atg11 were grown under respiratory conditions, the Atg32-Atg11 interaction brings the LgBiT and SmBiT subunits into close proximity, resulting in reversible reconstitution of an active luciferase that generates a luminescent signal in the presence of its substrate furimazine (Dixon et al., 2016) (Fig. S1 A). This system, which efficiently drives mitophagy (80% compared to wild-type cells) without overexpression, enables us to measure the resulting luminescent signals by a microplate reader and relatively quantify Atg32-Atg11 interactions *in*

vivo. Our NanoBiT system detected lower luminescent signals in cells lacking Get1, Get2, or Get3 (3-5-fold reduction compared to wild-type cells) under respiratory conditions (Fig. 1 C), indicating that Get components are required for promoting Atg32-Atg11 interactions.

Perturbation of the Ppg1 phosphatase restores Atg32-Atg11 interactions and mitophagy in get1/2-null cells

It is conceivable that a decrease in Atg32 phosphorylation causes suppression of Atg32-Atg11 interactions in cells lacking Get components (Fig. 1, A and C). Thus, we hypothesized that augmentation of Atg32 phosphorylation could rescue the impaired protein-protein interactions for mitophagy in GET-deficient cells. To test this possibility, we attempted to genetically increment Atg32 phosphorylation by loss of Ppg1, a protein phosphatase acting in dephosphorylation of Atg32 and suppression of Atg32-Atg11 interactions (Furukawa et al., 2018). Accordingly, we performed the NanoBiT assay and found that consistent with the previous report (Furukawa et al., 2018), loss of Ppg1 increased Atg32-Atg11 interactions (2-3-fold compared to wild-type cells) (Fig. 2 A). Remarkably, in *get1/2 ppg1*-double-null cells, Atg32 interacted with Atg11 at near wild-type levels, supporting the idea that reduced Atg32 phosphorylation in cells lacking Get1/2 is the primary cause of a defect in Atg32-Atg11 interactions (Fig. 2 A).

Next, we performed mitophagy assay using a mitochondrial matrix-localized DHFR-mCherry (mito-DHFR-mCherry) probe (Calvelli et al., 2020). When mitochondria are transported to the vacuole, DHFR-mCherry is processed by vacuolar proteases to generate free mCherry, enabling semi-quantitative detection of mitochondrial degradation. We confirmed that loss of Ppg1 accelerated mitophagy (137% compared to wild-type cells) (Fig. 2, B and C). Strikingly, *get1/ppg1*- and *get2/ppg1*-double-null cells exhibited mitophagy at near wild-type levels (112% and 89%, respectively, compared to wild-type cells) (Fig. 2, B and C). Moreover, expression of a

145 *PPG1 H111N* gene encoding a catalytically inactive phosphatase restored Atg32-Atg11
146 interactions and mitophagy in *get1/2*-null cells (Fig. S1, B-D). Together, these results suggest that
147 perturbation of Ppg1 increased the affinity of Atg32 for Atg11 in *get1/2*-null cells, thereby
148 recovering mitophagy.

149 To exclude the possibility that restoration of mitophagy in *get1/ppg1*- and *get2/ppg1*-double-
150 null cells is caused indirectly by pleiotropic alterations in Ppg1 substrate(s), we examined Atg32
151 variants lacking the amino acid residues 151-200 that are required for the Ppg1-Far complex to
152 interact with Atg32 (Furukawa et al., 2018; Innokentev et al., 2020). When this truncation was
153 introduced into the NanoBiT system, the Atg32 mutant (Δ151-200) interacted with Atg11 14-18-
154 fold more strongly than the full-length protein in the presence of Get1, and at near wild-type levels
155 even in the absence of Get1 (Fig. 2 D). Consistent with these results, mitophagy in *get1/2*-null
156 cells were mostly restored by expression of the Atg32 mutant (Δ151-200) (Fig. 2, E and F),
157 supporting the idea that Ppg1-Far-mediated suppression of Atg32-Atg11 interactions and
158 mitophagy is exacerbated in the absence of Get1/2.

159

160 ***The ER-resident Far complex predominantly targets to mitochondria in GET-deficient cells***

161 How could Ppg1 abrogate mitophagy in cells lacking Get1/2? It has been demonstrated that ER-
162 resident TA proteins localize to mitochondria in *get1/2*-null cells (Jonikas et al., 2009; Schuldiner
163 et al., 2008). In addition, Ppg1 interacts with the Far complex that acts in pheromone-induced cell
164 cycle arrest and the TORC2 signaling pathway (Furukawa et al., 2018; Kemp and Sprague, 2003;
165 Pracheil et al., 2012). Moreover, the Far complex contains the TA proteins Far9 and Far10, and is
166 anchored to the ER membrane in a manner dependent on their TA domains (Pracheil and Liu,
167 2013). Based on these findings, we hypothesized that disruption of the GET pathway may lead to
168 targeting of the ER-resident Ppg1-Far complex to the surface of mitochondria, thereby

oversuppressing mitophagy. To test this idea, Far8, a component of the Far complex, was functionally tagged with three copies of GFP, expressed from the chromosomal *FAR8* locus without overexpression, and observed using fluorescence microscopy. We found that Far8-3×GFP mostly colocalized with mCherry-tagged Sec63, an ER-anchored Hsp40/DnaJ family protein (Feldheim et al., 1992) that exhibited peripheral and perinuclear patterns, in wild-type cells under respiratory conditions (Fig. 3, A and B). By contrast, Far8-3×GFP predominantly localized to mitochondria in *get1*-null cells (93% of cells lacking Get1 and 9% of wild-type cells) (Fig. 3, C and D). We also confirmed that loss of Get2 or Get3 greatly increased mitochondria-targeted Far8-3×GFP (96% and 92% of *get2*- and *get3*-null cells, respectively) (Fig. S2 A).

To clarify whether the insertase activity of Get1/2 is required for Far8-3×GFP localization to the ER, we generated yeast strains expressing an inactive Get1 or Get2 variant with point mutations in their conserved cytosolic domain (Get1NRm: N72A, R73A, Get2RERRm: R14E, E15R, R16E, R17E) (Wang et al., 2011), and found that expression of these insertase-inactive mutants significantly disturbed ER localization of Far8-3×GFP (95% and 98% of cells expressing Get1NRm and Get2RERRm, respectively) (Fig. S2 B), further underscoring a primary role for the GET pathway in ER targeting of the Ppg1-Far complex. In cells expressing these mutants, mitophagy was moderately reduced (Fig. S2, C and D), indicating that the Get1/2 insertase activity is required for efficient mitophagy.

Since targeting of ER-resident TA proteins to the mitochondrial surface requires their TA domains (Farkas and Bohnsack, 2021), we assumed that loss of Far9 or Far10 could diminish mitochondrial localization of the Far complex in cells lacking Get1/2. In line with this idea, we found that Far8-3×GFP was hardly localized to mitochondria, but instead mostly dispersed throughout the cytoplasm (probably excluded from the vacuolar lumen) in *far9/10*-null, *far9/get1*- and *far10/get1*-double-null cells (Fig. 3, E and F), indicating that these TA proteins are

193 indispensable for targeting of the Far complex to the ER in wild-type cells or mitochondria in
194 GET-deficient cells.

195 It has recently been reported that a fraction of the Far complex is localized to mitochondria
196 even in wild-type cells under fermentable conditions (Innokentev et al., 2020). Although we
197 barely found mitochondrial localization of Far8-3×GFP under non-fermentable conditions (Fig.
198 3, A and C), it remained possible that a small fraction of the Far complex is localized to
199 mitochondria and degraded in a mitophagy-dependent manner. To clarify this issue, we performed
200 GFP-processing assays. Similar to mito-DHFR-mCherry, Far8-3×GFP localized to the ER and
201 mitochondria can be transported to the vacuole and processed to generate free GFP via ER-phagy
202 and mitophagy, respectively. Under respiratory conditions, generation of free GFP was reduced
203 by 50% in cells without mitophagy (*atg32*-null) or ER-phagy (*atg39/40*-double-null) (Mochida
204 et al., 2015) and 25% in cells without both events (*atg32/39/40*-triple-null) compared to wild-type
205 cells (Fig. S2, E and F). These results support the notion that a small fraction of the Ppg1-Far
206 complex escapes the GET pathway and localizes to the surface of mitochondria.
207
208 ***Loss of the Far9/10 TA proteins rescues mitophagic deficiencies in cells lacking Get1/2***
209 Our observations that mitochondrial localization of the Far complex in *get1*-null cells was
210 diminished by loss of Far9 or Far10 (Fig. 3, E and F) led us to examine Atg32-Atg11 interactions
211 and mitophagy in the absence of these TA proteins. Similar to the results obtained from *ppg1*-null
212 cells (Fig. 2, A-C), Atg32 interacted with Atg11 2-3-fold more strongly in cells lacking Far9 than
213 wild-type cells (Fig. 4 A). In addition, consistent with the previous findings (Furukawa et al.,
214 2018), mitophagy under respiratory conditions was increased in *far9*-null cells (139% compared
215 to wild-type cells) (Fig. 4, B and C). Strikingly, Atg32-Atg11 interactions and mitophagy were
216 restored at near wild-type levels in *get1/far9*- and *get2/far9*-double-null cells (Fig. 4, A-C).

Next, we investigated cells lacking Far10 and found only a slight and no increase in Atg32-Atg11 interactions and mitophagy (1.2-fold and 98%, respectively, compared to wild-type cells) (Fig. S3, A-C). Notably, *get1/far10*- and *get2/far10*-double-null cells exhibited a partial recovery in Atg32-Atg11 interactions (0.7- and 0.4-fold, respectively, compared to wild-type cells) (Fig. S3 A) and a substantial restoration in mitophagy (96% and 69%, respectively, compared to wild-type cells) (Fig. S3, B and C). Collectively, these data suggest that the Ppg1-Far complex is anchored to the mitochondrial surface via Far9/10 and acts in suppression of Atg32-Atg11 interactions and mitophagy.

Artificial ER anchoring of the Far complex increases Atg32-Atg11 interactions and mitophagy in get1/2-null cells

Based on our findings that loss of Get1/2 leads to excess mitochondrial localization of the Ppg1-Far complex (Fig. 3, A-D; and Fig. S2 A), we asked whether Get1/2-independent ER localization of the Ppg1-Far complex ameliorates mitophagy deficiencies in cells lacking Get1/2. To this end, the TA domain of Far9 was replaced with the TM domain (TM^{ER}) of Sec12, a single-pass ER membrane protein consisting of an N- and C-terminal domains facing the cytosol and ER lumen, respectively (d'Enfert et al., 1991). We confirmed that expression of Far9-TM^{ER} does not cause significant alterations in ER shape and Far8-3×GFP localizations (Fig. 5, A and B). As expected, Far8-3×GFP in cells expressing Far9-TM^{ER} was localized to the ER even in *get1/2*-null cells (Fig. 5, A and B; and Fig. S4, A and B). In addition, expression of Far9-TM^{ER} in cells lacking Get1/2 restored Atg32-Atg11 interactions at near wild-type levels (Fig. 5 C). Moreover, mitophagy was increased in *get1*- and *get2*-null cells (70% and 80%, respectively compared to wild-type cells) (Fig. 5, D and E), suggesting that ER retention of the Ppg1-Far complex is critical for efficient mitophagy.

241

242 ***Artificial mitochondrial anchoring of the Far complex partially reduces mitophagy***

243 As excess accumulation of the Far complex on the mitochondrial surface by loss of Get1/2 seems
244 to perturb mitophagy, we sought to test if artificial targeting of the Far complex to mitochondria
245 may suppress mitophagy without disrupting Get1/2 functions. The TA domains of Far9 and Far10
246 were replaced with those derived from Gem1 (Frederick et al., 2004), an OMM protein
247 (Far9/Far10-TA^{MITO}). We confirmed that Far8-3×GFP almost exclusively localizes to
248 mitochondria in cells expressing Far9/Far10-TA^{MITO} (Fig. 6, A and B). In these cells, mitophagy
249 under respiratory conditions was partially reduced (70% compared to wild-type cells) (Fig. 6, C
250 and D). Importantly, this reduction was mostly abrogated in cells expressing Ppg1^{H111N}, a
251 catalytically inactive mutant (Fig. S5, A and B), suggesting that mitophagy suppression by the
252 OMM-anchored Far complex requires Ppg1 phosphatase activity.

253

254 ***Msp1 is required for efficient mitophagy in cells lacking Get3***

255 Previous studies demonstrate that Msp1, an OMM-anchored AAA-ATPase acting as an extractase,
256 is important to remove non-mitochondrial TA proteins from the surface of mitochondria in the
257 absence of Get components (Chen et al., 2014; Okreglak and Walter, 2014; Wang et al., 2020).
258 Accordingly, we asked whether loss of Msp1 exacerbates mitophagy deficiencies in cells lacking
259 the GET pathway. As double knockout of Msp1 and Get1/2 elicited extremely severe growth
260 defects under respiratory conditions, we performed fluorescence microscopy and mitophagy
261 assays for *msp1/get3*-double-null cells that could grow slowly with relatively mild phenotypes in
262 liquid non-fermentable medium. Single knockout of Msp1 and Get3 slightly affected mitophagy
263 (85% and 93%, respectively, compared to wild-type cells), whereas loss of these two proteins
264 significantly compromised mitophagy (48% compared to wild-type cells) (Fig. 7, A and B). In

addition, loss of Get3 in cells expressing Msp1^{E193Q} (Msp1EQ, an ATPase-inactive mutant) also synergistically disturbed degradation of mitochondria (51% compared to wild-type cells) (Fig. 7, A and B). These results suggest that Msp1 ATPase activity is critical to prevent mitophagy suppression in GET-deficient cells.

Next, we performed fluorescence microscopy and found that loss of Msp1 did not significantly affect ER localization of Far8-3×GFP (Fig. 7, C and D). By contrast, Far8-3×GFP localized to mitochondria in *get3*-null and *msp1/get3*-double-null cells (Fig. 7, C and D). Based on these observations, we investigated if loss of Ppg1 affects mitophagy in *msp1*/*get3*-double-null cells, and found that *msp1/get3/ppg1*-triple-null cells significantly restored mitophagy (81% compared to wild-type cells) (Fig. 7, E and F). Similarly, expression of Atg32(Δ151-200), a deletion mutant lacking a domain required for Ppg1-mediated dephosphorylation, also increased mitophagy in cells lacking Get3 and Msp1 (60% compared to wild-type cells) (Fig. S5, C and D). Collectively, these results support the idea that the GET pathway and Msp1 cooperatively act to prevent suppression of mitophagy by the Ppg1-Far complex.

Discussion

In the present study, we show that the GET pathway contributes to Atg32 phosphorylation by promoting localization of the Ppg1-Far phosphatase complex to the ER (Fig. 8). Loss of Get1/2 (ER membrane-anchored insertase), or Get3 (cytosolic ATPase), partially reduces Atg32 phosphorylation, thereby abrogating Atg32-Atg11 interactions in the early phase of respiratory growth (Fig. 1, A and C). Consistent with this observation, mitophagy is severely compromised in *get1/2*-null cells under prolonged respiration (Onishi et al., 2018). However, cells lacking Get3 exhibit only minor defects in mitophagy (Onishi et al., 2018), raising the possibility that in the prolonged phase of respiratory growth, Get1/2 may have unappreciated additional function(s) to

289 promote mitophagy independently of its insertase activity (Fig. S2, B-D), or that unknown
290 protein(s) may exert a Get3-related compensatory role in promoting mitophagy.

291 Evidently, Atg32-Atg11 interactions and mitophagy in cells lacking Get1/2 can mostly be
292 restored by additional loss of Ppg1, a phosphatase that dephosphorylates Atg32 (Fig. 2, A-F),
293 suggesting that Ppg1 is likely to be the primary cause of reduced Atg32 phosphorylation in *get1/2*-
294 null mutants. Consistent with these findings, loss of Far9, a component of the Far complex that
295 binds to Ppg1 and acts in a cooperative manner to dephosphorylate Atg32, also increased Atg32-
296 Atg11 interactions and mitophagy in Get1/2-deficient cells (Fig. 4, A-C). Far9 is an ER-resident
297 TA protein of the Far complex (Pracheil and Liu, 2013), and loss of the Get1/2 insertase activity
298 perturbs ER localization of the Far complex (Fig. 3, A-D; and Fig. S2, A and B), supporting the
299 idea that the GET pathway promotes insertion of the Far TA proteins to the ER membrane.

300 Although disruption of the GET pathway leads to targeting of multiple ER-resident TA proteins
301 to mitochondria (Jonikas et al., 2009; Schuldiner et al., 2008), how these ectopically targeted
302 proteins impact events on the mitochondrial surface remains enigmatic. Upon loss of Get
303 components, the Far complex predominantly targets to mitochondria (Fig. 3, A-D; and Fig. S2, A
304 and B) in a manner dependent on the TA proteins Far9 and Far10 (Fig. 3, E and F). Anchoring to
305 the mitochondrial surface seems to be critical for the Far complex to efficiently abrogate Atg32-
306 Atg11 interactions and mitophagy, since cytosolic diffusion or GET-independent ER anchoring
307 of the Far complex leads to restoration of those processes in *get1/2*-null cells (Fig. 4, A-C; and
308 Fig. S3, A-C; and Fig. 5, C-E). Based on the observations from us (Fig. S2, E and F) and others
309 (Innokentev et al., 2020) that a fraction of the Far complex localizes to mitochondria even in wild-
310 type cells, we favor a hypothetical model that dynamic changes in the GET pathway (*e.g.*
311 expression level, insertase activity, and substrate affinity) could affect the number of Ppg1-Far
312 complex targeted to the ER or mitochondria, thereby serving as a regulatory process for

mitophagy (Fig. 8). Further studies are needed to test this hypothesis.

During the course of this study, we noticed that our several results seem to be somewhat different from the recently reported data on localization and function of the Ppg1-Far complex (Innokentev et al., 2020). First, we demonstrate that the Far complex is mostly localized to the ER in cells during non-fermentable growth (Fig. 3 A-D), whereas it has been shown that the Far complex is distributed almost equally to both mitochondria and the ER in cells during fermentable growth (Innokentev et al., 2020). These distinct features might be due to different growth condition (mitophagy-inducing or -noninducing). Second, cells containing the GET-independently ER-localized Far complex exhibit mitophagy at near wild-type levels under prolonged respiration (Fig. 5, D and E), whereas cells containing the Far9-Cyb5^{TA}-dependently ER-localized Far complex have been shown to accelerate mitophagy at the early stationary phase (Innokentev et al., 2020). These differences might result from TM segments (one derived from the non-TA protein Sec12 or TA protein Cyb5) and/or mitophagy assay time points (72 h or 40 h in non-fermentable medium). Third, we show that Gem1 TA-dependent artificial targeting of the Far complex to mitochondria causes a partial defect in mitophagy under prolonged respiration (Fig. 6, C and D), whereas it has been demonstrated that mitochondria-targeted Far complex by Tom5 TA strongly diminishes mitophagy at the early stationary phase (Innokentev et al., 2020). This phenotypic difference might be attributed to TA domains used for mitochondrial anchoring and/or mitophagy assay time points (72 h or 40 h in non-fermentable medium). Nevertheless, it seems possible that the mitochondria-anchored Ppg1-Far complex could suppress stationary-phase mitophagy more effectively at the early phase than the late phase.

Expression of the Get1/2 insertase-inactive mutants leads to extensive accumulation of the Ppg1-Far complex on the mitochondrial surface, while mitophagy is only partially decreased in these mutant cells (70% compared to wild-type cells) (Fig. S2, B-D). Notably, these phenotypes

337 are similar to those in *get3*-null cells (Fig. 7, A-D) (Onishi et al., 2018), which is in agreement
338 with the previous finding that the Get1/2 insertase-inactive mutants cannot recruit Get3 to the ER
339 (Wang et al., 2011). In addition, artificial targeting of the Ppg1-Far complex to mitochondria only
340 partially reduces mitophagy under prolonged respiration (70% compared to wild-type cells) (Fig.
341 6, C and D). Together, these findings raise the possibility that Get1/2 may be a bifunctional
342 complex acting as a general insertase for ER-resident TA proteins, and serving as a pro-
343 mitophagic factor independently of its insertase activity.

344 Finally, our data reveal a potential role of the OMM-anchored AAA-ATPase Msp1 in
345 mitophagy. Consistent with the previous reports that Msp1 extracts non-mitochondrial TA
346 proteins from the mitochondrial surface upon loss of Get components (Chen et al., 2014; Okreglak
347 and Walter, 2014; Wang et al., 2020; Wohlever et al., 2017), cells lacking both Get3 and Msp1
348 display synthetic defects in mitophagy that can be rescued by loss of Ppg1 or expression of an
349 Atg32 variant defective for interaction with the Ppg1-Far complex (Fig. 7, A and B, E and F; and
350 Fig. S5, C and D). Thus, although ER localization of the Far complex seems to be hardly altered
351 in cells lacking Msp1 (Fig. 7, C and D), it remains possible that this OMM-anchored extractase
352 may act in removal of non-mitochondrial TA proteins, such as Far9 and Far10, thereby
353 contributing to Atg32 phosphorylation, Atg32-Atg11 interactions, and mitophagy (Fig. 8). How
354 the GET pathway and Msp1 coordinately act in activation of Atg32-mediated mitophagy awaits
355 further investigations.

356

357 **Materials and methods**

358 **Yeast strains and plasmids used in this study**

359 Yeast strains and plasmids used in this thesis are listed in Table S1 and S2. Standard genetic and
360 molecular biology methods were performed for generating yeast strains.

361

362 **Growth conditions of yeast**

363 Yeast cells were incubated in YPD medium (1% yeast extract, 2% peptone and 2% dextrose),
364 synthetic medium (0.17% yeast nitrogen base without amino acids and ammonium sulfate, 0.5%
365 ammonium sulfate) with 0.5% casamino acids and either 2% dextrose (SDCA), or 0.1% dextrose
366 plus 3% glycerol (SDGCA), supplemented with the necessary amino acids. For mitophagy assay
367 under respiratory conditions, cells grown to mid-log phase in SDCA were transferred to SDGCA
368 and incubated at 30ºC.

369

370 **Protein phosphatase treatment assays**

371 For protein phosphatase assays, cells were pre-grown in SDCA, and transferred to SDGCA. 2.0
372 OD_{600} units of cells were collected and subjected to alkaline lysis and TCA (Trichloroacetic acid)
373 precipitation. The pellet was resuspended in a reaction buffer (50 mM Tris-HCl pH 7.5, 100 mM
374 NaCl, 2 mM DTT, 0.5 mM EDTA, 0.01% Brij-35, 2 mM MgCl2), treated with or without lambda
375 protein phosphatase (λ-PPase) in the presence or absence of PPase inhibitor at 30℃ for 1 h.
376 Samples corresponding to 0.2 OD_{600} units of cells were loaded per lane

377

378 **Structured illumination microscopy**

379 Live yeast cells expressing Far8-3×GFP were observed using a structured illumination
380 microscopy (Stefer et al.). Differential interference contrast (DIC) and fluorescence images were
381 obtained under a KEYENCE BZ-X810 system equipped with a 100× objective lens (CFI
382 Apochromat TIRF 100XC Oil, Plan-APO TIRF 100, NA: 1.49; Nikon), filter sets for GFP and
383 mCherry (BZ-X filter GFP and BZ-X filter TRITC, respectively; KEYENCE). Cell images were
384 captured using acquisition and analysis software (BZ-X800 Analyzer; KEYENCE).

385

386 **Western blotting**

387 Samples corresponding to 0.1-0.4 OD600 units of cells were separated by SDS-PAGE followed
388 by western blotting and immunodecoration with primary antibodies raised against mCherry
389 (1:2,000, Abcam ab125096), Pgk1 (1:10,000, Abcam, ab113687), GFP (1:1000, Roche,
390 13921700), HA (1:5,000, Sigma, A2095). After treatment with the secondary antibodies,
391 horseradish peroxidase (HRP)-conjugated rabbit anti-mouse IgG (H + L) for mCherry, GFP, HA,
392 Pgk1, followed by the enhanced chemiluminescence reagent Western Lightning Plus-ECL
393 (PerkinElmer, 203-19151) or ImmunoStar LD (Wako, PTJ2005), proteins were detected using a
394 luminescent image analyzer (FUSION Solo S; VILBER). Quantification of the signals was
395 performed using FUSION Solo S (VILBER).

396

397 **Bioluminescence assay for protein-protein interactions**

398 For quantitative analysis of Atg32-Atg11 interactions using NanoLuc Binary Technology
399 (NanoBiT, Promega), Atg32 fused to 3 copies of GFP and Large BiT (LgBiT; 17.6 kDa), and
400 Atg11 fused to Small BiT (SmBiT; 11 amino acids) were expressed endogenously (constructed
401 by Yang Liu, Osaka University, Japan). Upon interaction of Atg32 and Atg11 with each other,
402 SmBiT and LgBiT are brought into close proximity, leading to structural complementation and
403 generation of a luminescent signal. For the assay, cells were grown in glycerol media (SDGCA).
404 1.0 OD600 units of cells were collected in the early phase of respiration (OD600: 1.4~1.6) and
405 washed with 400 µl PBS. After washing, cells were dissolved in 40 µl PBS and applied to a 96
406 well plate. The detection reagent was prepared by diluting the Nano-Glo Live Cell Substrate
407 (Promega, 0000360026) with the Nano-Glo LCS Dilution Buffer (Promega, 0000333050) to
408 make the Nano-Glo Live Cell Reagent. 10 µl diluted detection reagent was added onto the 96 well

409 plate and mixed with the cells. Then, cells were incubated at 37°C for 1 hour. After incubation,
410 the luminescent signal was detected by the microplate reader (Fluoroskan Ascent FL; Thermo
411 Fisher Scientific) (exposure time: 1,000 ms). For the detection of the GFP fluorescent signal
412 derived from Atg32, 1.0 OD_{600} units of cells were collected at the same time point, and dissolved
413 in 100 µl SDGCA media, applied to the 96 well plate. GFP signal was measured by microplate
414 reader (Fluoroskan Ascent FL; Thermo Fisher Scientific) (excitation: 485 nm, emission: 538 nm,
415 exposure time: 1,000 ms), and used to normalize the luminescence intensity.
416
417 **Statistical analysis**
418 Results are presented as means including ± standard deviation. Statistical analyses were
419 performed with Excel for Mac (Microsoft) and GraphPad Prism 9 (GraphPad Software), using
420 two-tailed Student's *t*-test and one-way ANOVA followed by Tukey's or Dunnett's multiple
421 comparison test. All the statistical tests performed are indicated in the figure legends.
422
423 **Online supplemental material**
424 Fig. S1 shows a schematic description on the NanoBiT assays for Atg32-Atg11 interactions, and
425 the results on Atg32-Atg11 interactions and mitophagy in *get1/2*-null cells expressing a
426 catalytically inactive Ppg1 mutant. Fig. S2 contains the data from microscopic imaging,
427 mitophagy assay, and processing assay for cells expressing Far8-3×GFP and mito-DHFR-
428 mCherry. Fig. S3 shows the results on Atg32-Atg11 interactions and mitophagy in *get1/2*-null
429 cells lacking Far10. Fig. S4 contains the data from microscopic imaging for *get1/2*-null cells
430 expressing an artificially ER-anchored Far9. Fig. S5 shows the results on mitophagy in cells
431 expressing a catalytically inactive Ppg1 mutant and an ectopically mitochondria-targeted Far9/10.
432 Table S1 contains a list of yeast strains used in this study. Table S2 shows a list of plasmid used

in this study.

Acknowledgements

We thank Miyuki Sato (Gunma University, Japan) for valuable suggestions on artificial ER anchoring, Elmar Schiebel (Heidelberg University, Germany) for kindly providing us with the plasmid pFA6a-3myeGFP-kanMX6, and Yang Liu (Osaka University, Japan) for providing us with the NanoBiT assay strains. This work was supported in part by JSPS KAKENHI Grants JP19J10384, JP21K15041 (to M.O.), JP16H04784, JP19H03222, and JP20H05324 (to KO), and the Osaka University International Joint Research Promotion Programs (Type A+ and Type A-GKP) (to KO).

The authors declare no competing financial interests.

Author contributions: M. Onishi and K. Okamoto obtained funding and conceptualized the study. M. Onishi and K. Okamoto designed experiments. M. Onishi performed experiments. M. Onishi and K. Okamoto wrote the manuscript.

References

Aoki, Y., T. Kanki, Y. Hirota, Y. Kurihara, T. Saigusa, T. Uchiumi, and D. Kang. 2011. Phosphorylation of Serine 114 on Atg32 mediates mitophagy. *Mol. Biol. Cell*. 22:3206-3217.

Barlowe, C.K., and E.A. Miller. 2013. Secretory protein biogenesis and traffic in the early secretory pathway. *Genetics*. 193:383-410.

Bozkurt, G., G. Stjepanovic, F. Vilardi, S. Amlacher, K. Wild, G. Bange, V. Favaloro, K. Rippe, E. Hurt, B. Dobberstein, and I. Sinning. 2009. Structural insights into tail-anchored protein

457 binding and membrane insertion by Get3. *Proc. Natl. Acad. Sci. U S A*. 106:21131-21136.

458 Calvelli, H., J. Krigman, M. Onishi, D.P. Narendra, N. Sun, and K. Okamoto. 2020. Detection of
459 mitophagy in mammalian cells, mice, and yeast. *Methods Cell Biol*. 155:557-579.

460 Chen, Y.C., G.K. Umanah, N. Dephoure, S.A. Andrabi, S.P. Gygi, T.M. Dawson, V.L. Dawson,
461 and J. Rutter. 2014. Msp1/ATAD1 maintains mitochondrial function by facilitating the
462 degradation of mislocalized tail-anchored proteins. *EMBO J*. 33:1548-1564.

463 d'Enfert C, C. Barlowe, S. Nishikawa, A. Nakano, R. Schekman. 1991. Structural and functional
464 dissection of a membrane glycoprotein required for vesicle budding from the endoplasmic
465 reticulum. *Mol Cell Biol.* 11:5727-5734.

466 Denic, V. 2012. A portrait of the GET pathway as a surprisingly complicated young man. *Trends*
467 *Biochem. Sci*. 37:411-417.

468 Denic, V., V. Dotsch, and I. Sinning. 2013. Endoplasmic reticulum targeting and insertion of tail-
469 anchored membrane proteins by the GET pathway. *Cold Spring Harb. Perspect. Biol*.
470 5:a013334.

471 Dixon, A.S., M.K. Schwinn, M.P. Hall, K. Zimmerman, P. Otto, T.H. Lubben, B.L. Butler, B.F.
472 Binkowski, T. Machleidt, T.A. Kirkland, M.G. Wood, C.T. Eggers, L.P. Encell, and K.V.
473 Wood. 2016. NanoLuc complementation reporter optimized for accurate measurement of
474 protein interactions in cells. *ACS. Chem. Biol*. 11:400-408.

475 Farkas, A., and K.E. Bohnsack. 2021. Capture and delivery of tail-anchored proteins to the
476 endoplasmic reticulum. *J. Cell Biol*. 220:e202105004.

477 Feldheim D, J. Rothblatt, and R. Schekman. 1992. Topology and functional domains of Sec63p,
478 an endoplasmic reticulum membrane protein required for secretory protein translocation. *Mol*
479 *Cell Biol.* 12:3288-3296.

480 Frederick, R.L., J.M. McCaffery, K.W. Cunningham, K. Okamoto, and J.M. Shaw. 2004. Yeast

Miro GTPase, Gem1p, regulates mitochondrial morphology via a novel pathway. *J. Cell Biol*. 167:87-98.

Furukawa, K., T. Fukuda, S. Yamashita, T. Saigusa, Y. Kurihara, Y. Yoshida, H. Kirisako, H. Nakatogawa, and T. Kanki. 2018. The PP2A-like protein phosphatase Ppg1 and the Far complex cooperatively counteract CK2-mediated phosphorylation of Atg32 to inhibit mitophagy. *Cell Rep*. 23:3579-3590.

He, C., H. Song, T. Yorimitsu, I. Monastyrska, W.L. Yen, J.E. Legakis, and D.J. Klionsky. 2006. Recruitment of Atg9 to the preautophagosomal structure by Atg11 is essential for selective autophagy in budding yeast. *J. Cell Biol*. 175:925-935.

Innokentev, A., K. Furukawa, T. Fukuda, T. Saigusa, K. Inoue, S.I. Yamashita, and T. Kanki. 2020. Association and dissociation between the mitochondrial Far complex and Atg32 regulate mitophagy. *elife*. 9:e63694.

Jonikas, M., S. Collins, V. Denic, E. Oh, E. Quan, V. Schmid, J. Weibezahn, B. Schwappach, P. Walter, J. Weissman, and M. Schuldiner. 2009. Comprehensive characterization of genes required for protein folding in the endoplasmic reticulum. *Science*. 323:1693–1697.

Kanki, T., Y. Kurihara, X. Jin, T. Goda, Y. Ono, M. Aihara, Y. Hirota, T. Saigusa, Y. Aoki, T. Uchiumi, and D. Kang. 2013. Casein kinase 2 is essential for mitophagy. *EMBO Rep*. 14:788-794.

Kanki, T., K. Wang, Y. Cao, M. Baba, and D.J. Klionsky. 2009. Atg32 is a mitochondrial protein that confers selectivity during mitophagy. *Dev. Cell*. 17:98-109.

Kemp, H.A., and G.F. Sprague, Jr. 2003. Far3 and five interacting proteins prevent premature recovery from pheromone arrest in the budding yeast *Saccharomyces cerevisiae*. *Mol. Cell Biol*. 23:1750-1763.

Kondo-Okamoto, N., N.N. Noda, S.W. Suzuki, H. Nakatogawa, I. Takahashi, M. Matsunami, A.

505 Hashimoto, F. Inagaki, Y. Ohsumi, and K. Okamoto. 2012. Autophagy-related protein 32 acts
506 as autophagic degron and directly initiates mitophagy. *J. Biol. Chem*. 287:10631-10638.
507 Mao, K., L.H. Chew, Y. Inoue-Aono, H. Cheong, U. Nair, H. Popelka, C.K. Yip, and D.J.
508 Klionsky. 2013. Atg29 phosphorylation regulates coordination of the Atg17-Atg31-Atg29
509 complex with the Atg11 scaffold during autophagy initiation. *Proc. Natl. Acad. Sci. U S A*.
510 110:E2875-2884.
511 Mateja, A., M. Paduch, H. Chang, A. Szydlowska, A. Kossiakoff, R. Hegde, and R. Keenan. 2015.
512 Structure of the Get3 targeting factor in complex with its membrane protein cargo. *Science*.
513 347:1152-1155.
514 Mateja, A., A. Szlachcic, M.E. Downing, M. Dobosz, M. Mariappan, R.S. Hegde, and R.J.
515 Keenan. 2009. The structural basis of tail-anchored membrane protein recognition by Get3.
516 *Nature*. 461:361-366.
517 McDowell, M.A., M. Heimes, F. Fiorentino, S. Mehmood, A. Farkas, J. Coy-Vergara, D. Wu,
518 J.R. Bolla, V. Schmid, R. Heinze, K. Wild, D. Flemming, S. Pfeffer, B. Schwappach, C.V.
519 Robinson, and I. Sinning. 2020. Structural basis of tail-anchored membrane protein biogenesis
520 by the GET insertase complex. *Mol. Cell*. 80:72-86.e7.
521 Mochida, K., Y. Oikawa, Y. Kimura, H. Kirisako, H. Hirano, Y. Ohsumi, and H. Nakatogawa.
522 2015. Receptor-mediated selective autophagy degrades the endoplasmic reticulum and the
523 nucleus. *Nature*. 522:359-362.
524 Okamoto, K., N. Kondo-Okamoto, and Y. Ohsumi. 2009. Mitochondria-anchored receptor Atg32
525 mediates degradation of mitochondria via selective autophagy. *Dev. Cell*. 17:87-97.
526 Okreglak, V., and P. Walter. 2014. The conserved AAA-ATPase Msp1 confers organelle
527 specificity to tail-anchored proteins. *Proc. Natl. Acad. Sci. U S A*. 111:8019-8024.
528 Onishi, M., S. Nagumo, S. Iwashita, and K. Okamoto. 2018. The ER membrane insertase Get1/2

529 is required for efficient mitophagy in yeast. *Biochem. Biophys. Res. Commun*. 503:14-20.

530 Onishi, M., and K. Okamoto. 2021. Mitochondrial clearance: mechanisms and roles in cellular
531 fitness. *FEBS Lett*. 595:1239-1263.

532 Onishi, M., K. Yamano, M. Sato, N. Matsuda, and K. Okamoto. 2021. Molecular mechanisms
533 and physiological functions of mitophagy. *EMBO J.* 40:e104705.

534 Palikaras, K., E. Lionaki, and N. Tavernarakis. 2018. Mechanisms of mitophagy in cellular
535 homeostasis, physiology and pathology. *Nat. Cell Biol*. 20:1013-1022.

536 Pracheil, T., and Z. Liu. 2013. Tiered assembly of the yeast Far3-7-8-9-10-11 complex at the
537 endoplasmic reticulum. *J. Biol. Chem.* 288:16986-16997.

538 Pracheil, T., J. Thornton, and Z. Liu. 2012. TORC2 signaling is antagonized by protein
539 phosphatase 2A and the Far complex in *Saccharomyces cerevisiae*. *Genetics*. 190:1325-1339.

540 Schuldiner, M., J. Metz, V. Schmid, V. Denic, M. Rakwalska, H.D. Schmitt, B. Schwappach, and
541 J.S. Weissman. 2008. The GET complex mediates insertion of tail-anchored proteins into the
542 ER membrane. *Cell*. 134:634-645.

543 Stefer, S., S. Reitz, F. Wang, K. Wild, Y. Pang, D. Schwarz, J. Bomke, C. Hein, F. Löhr, F.
544 Bernhard, V. Denic, V. Dötsch, and I. Sinning. 2011. Structural basis for tail-anchored
545 membrane protein biogenesis by the Get3-receptor complex. *Science*. 333:758-762.

546 Suloway, C.J., J.W. Chartron, M. Zaslaver, and W.M. Clemons, Jr. 2009. Model for eukaryotic
547 tail-anchored protein binding based on the structure of Get3. *Proc. Natl. Acad. Sci. U S A*.
548 106:14849-14854.

549 Wang, F., C. Chan, N.R. Weir, and V. Denic. 2014. The Get1/2 transmembrane complex is an
550 endoplasmic-reticulum membrane protein insertase. *Nature*. 512:441-444.

551 Wang, F., A. Whynot, M. Tung, and V. Denic. 2011. The mechanism of tail-anchored protein
552 insertion into the ER membrane. *Mol. Cell*. 43:738-750.

553 Wang, L., A. Myasnikov, X. Pan, and P. Walter. 2020. Structure of the AAA protein Msp1 reveals
554 mechanism of mislocalized membrane protein extraction. *elife*. 9:e54031.
555 Wohlever, M.L., A. Mateja, P.T. McGilvray, K.J. Day, and R.J. Keenan. 2017. Msp1 is a
556 membrane protein dislocase for tail-anchored proteins. *Mol. Cell*. 67:194-202.e6.
557 Yamagata, A., H. Mimura, Y. Sato, M. Yamashita, A. Yoshikawa, and S. Fukai. 2010. Structural
558 insight into the membrane insertion of tail-anchored proteins by Get3. *Genes Cells*. 15:29-41.
559 Zhang, J., Y. Wang, Z. Chi, M.J. Keuss, Y.M. Pai, H.C. Kang, J.H. Shin, A. Bugayenko, H. Wang,
560 Y. Xiong, M.V. Pletnikov, M.P. Mattson, T.M. Dawson, and V.L. Dawson. 2011. The AAA+
561 ATPase Thorase regulates AMPA receptor-dependent synaptic plasticity and behavior. *Cell*.
562 145:284-299.
563
564
565
566
567
568
569
570
571
572
573
574
575
576

Figure legends

Figure 1. **Atg32 phosphorylation and Atg32-Atg11 interactions are reduced in cells lacking Get components. (A)** Wild-type, *get1Δ*, *get2Δ*, and *get3*Δ cells containing a plasmid encoding Atg32-3HAn (p-*ATG32-3HAn*) grown in fermentable dextrose medium (Dex) were cultured in non-fermentable glycerol medium (Gly), collected at the indicated OD_{600} points, and subjected to western blotting. All strains are *pep4/prb1/atg32*-triple-null derivatives defective in vacuolar degradation of Atg32-3HAn via mitophagy. Atg32 is phosphorylated at the early stages of respiratory growth, and phosphorylated Atg32 molecules are detected as multiple upper protein bands. Orange arrowheads and dots indicate putative phosphorylated Atg32. Pgk1 was monitored as a loading control. **(B)** *pep4*Δ *prb1*Δ *atg32*Δ and *pep4*Δ *prb1*Δ *atg32*Δ *get1*Δ cells containing a plasmid encoding Atg32-HAn were grown in glycerol medium, collected at the OD_{600} = 2.5 point, and subjected to alkaline lysis and TCA precipitation. The pellet was resuspended in a reaction buffer, treated with or without lambda protein phosphatase (λ-PPase) in the presence or absence of PPase inhibitor. **(C)** Wild-type, *get1*Δ, *get2*Δ and *get3*Δ cells expressing Atg32 internally tagged with 3×GFP plus Large BiT (LgBiT) and Atg11 C-terminally tagged with Small BiT (SmBiT) or wild-type cells expressing Atg32 and Atg11 (negative control, N.C.), were grown in glycerol medium, collected at the OD_{600} = 1.4 point, incubated with substrates, and subjected to the NanoBiT-based bioluminescence assay. Data represent the averages of all experiments, with bars indicating standard deviations (n = 5 independent cultures). Data were analyzed by one-way analysis of variance (ANOVA) with Dunnett's multiple comparison test.

Figure 2. **Perturbation of the Ppg1 phosphatase restores Atg32-Atg11 interactions and mitophagy in *get1/2*-null cells. (A)** Wild-type, *ppg1*Δ, *get1*Δ, *get2*Δ, *get1*Δ *ppg1*Δ, and *get2*Δ *ppg1*Δ cells expressing Atg32-3HA-3×GFP-3FLAG-LgBiT and Atg11-HA-SmBiT, or wild-type

cells expressing Atg32 and Atg11 (negative control, N.C.) were grown in glycerol medium (Gly), collected at the OD_{600} = 1.4 point, incubated with substrates, and subjected to the NanoBiT-based bioluminescence assay. Data represent the averages of all experiments, with bars indicating standard deviations (n = 3 independent cultures). **(B)** Wild-type, *ppg1*Δ, *get1*Δ, *get2*Δ, *get1*Δ *ppg1*Δ, *get2*Δ *ppg1*Δ, and *atg32*Δ cells expressing mitochondrial matrix-targeted DHFR-mCherry (mito-DHFR-mCherry) were grown in glycerol medium (Gly), collected at the indicated time points, and subjected to western blotting. Generation of free mCherry indicates transport of mitochondria to the vacuole. **(C)** The amounts of free mCherry in cells analyzed in **(B)** was quantified in three experiments. The signal intensity value of free mCherry in wild-type cells at the 72 h time point was set to 100%. Data represent the averages of all experiments, with bars indicating standard deviations (n = 3 independent cultures). **(D)** Wild-type and *get1*Δ cells expressing Atg11-HA-SmBiT and Atg32-3HA-3×GFP-3FLAG-LgBiT or (Δ151-200)-3HA-3×GFP-3FLAG-LgBiT, or wild-type cells expressing Atg32 and Atg11 (negative control, N.C.) were grown in glycerol medium (Gly), collected at the OD_{600} = 1.4 point, incubated with substrates, and subjected to the NanoBiT-based bioluminescence assay. Data represent the averages of all experiments, with bars indicating standard deviations (n = 3 independent cultures). **(E)** Wild-type, *get1*Δ, and *get2*Δ cells expressing chromosomally integrated *ATG32* wild-type or *ATG32 (Δ151-200)* were grown in glycerol medium (Gly), collected at the indicated time points, and subjected to western blotting. **(F)** The amounts of free mCherry in cells analyzed in **(E)** was quantified in four experiments. The signal intensity value of free mCherry in wild-type cells at the 72 h time point was set to 100%. Data represent the averages of all experiments, with bars indicating standard deviations (n = 4 independent cultures). Data were analyzed by two-tailed Student's t test **(A, C, D, F)**.

Figure 3. **The ER-resident Far complex predominantly targets to mitochondria in GET-deficient cells. (A)** Representative images of wild-type and *get1*Δ cells expressing Sec63-mCherry and Far8-3×GFP grown for 24 h in glycerol medium (Gly) and observed by structured illumination microscopy. Arrowheads indicate Far8-3×GFP localized to mitochondria. Scale bar, 2 μm. DIC, differential interference contrast. **(B)** Cells analyzed in **(A)** were quantified in three experiments. Data represent the averages of all experiments, with bars indicating standard deviations (n = 3 independent cultures). **(C)** Representative images of wild-type and *get1*Δ cells expressing mito-DHFR-mCherry and Far8-3×GFP grown for 24 h in glycerol medium (Gly) and observed by structured illumination microscopy. Scale bar, 2 μm. **(D)** Cells analyzed in **(C)** were quantified in three experiments. Data represent the averages of all experiments, with bars indicating standard deviations (n = 3 independent cultures). **(E)** Representative images of wild-type, *far9*Δ, *far10*Δ, *get1*Δ, *get1*Δ *far9*Δ, and *get1*Δ *far10*Δ cells expressing Sec63-mCherry and Far8-3×GFP3 grown for 24 h in glycerol medium (Gly) and observed by structured illumination microscopy. Scale bar, 2 μm. **(F)** Cells analyzed in **(E)** were quantified in three experiments. Data represent the averages of all experiments, with bars indicating standard deviations. Data were analyzed by two-tailed Student's t test **(B, D)**.

Figure 4. **Loss of the Far9/10 TA proteins rescues mitophagic deficiencies in cells lacking Get1/2. (A)** Wild-type, *far9*Δ, *get1*Δ, *get2*Δ, *get1*Δ *far9*Δ, and *get2*Δ *far9*Δ cells expressing Atg32-3HA-3×GFP-3FLAG-LgBiT and Atg11-HA-SmBiT, or wild-type cells expressing Atg32 and Atg11 (negative control, N.C.) were grown in glycerol medium (Gly), collected at the OD_{600} = 1.4 point, incubated with substrates, and subjected to the NanoBiT-based bioluminescence assay. Data represent the averages of all experiments, with bars indicating standard deviations (n = 3 independent cultures). **(B)** Wild-type, *far9*Δ, *get1*Δ, *get2*Δ, *get1*Δ*far9*Δ, *get2*Δ *far9*Δ, and *atg32*Δ

649 cells expressing mito-DHFR-mCherry were grown in glycerol medium (Gly), collected at the
650 indicated time points, and subjected to western blotting. **(C)** The amounts of free mCherry in cells
651 analyzed in **(B)** was quantified in three experiments. The signal intensity value of free mCherry
652 in wild-type cells at the 72 h time point was set to 100%. Data represent the averages of all
653 experiments, with bars indicating standard deviations (n = 3 independent cultures). Data were
654 analyzed by two-tailed Student's t test **(A, C)**.
655
656 Figure 5. **Artificial ER anchoring of the Far complex increases Atg32-Atg11 interactions and**
657 **mitophagy in *get1/2*-null cells. (A)** Representative images of wild-type, *get1*Δ, and *get2*Δ cells
658 expressing the endogenous Far9 or a variant whose TA domain was replaced with the Sec12 TM
659 domain (*FAR9-TM*^{ER}) grown for 24 h in glycerol medium (Gly) and observed by structured
660 illumination microscopy. All strains were derivatives expressing Sec63-mCherry and Far8-3×GFP.
661 Scale bar, 2 μm. **(B)** Cells analyzed in **(A)** were quantified in three experiments. Data represent
662 the averages of all experiments, with bars indicating standard deviations (n = 3 independent
663 cultures). **(C)** Derivatives of cells analyzed in **(D)** expressing Atg32-3HA-3×GFP-3FLAG-LgBiT
664 and Atg11-HA-SmBiT, or wild-type cells expressing Atg32 and Atg11 (negative control, N.C.),
665 were grown in glycerol medium (Gly), collected at the OD_{600} = 1.4 point, incubated with
666 substrates, and subjected to the NanoBiT-based bioluminescence assay. Data represent the
667 averages of all experiments, with bars indicating standard deviations (n = 4 independent cultures).
668 **(D)** Wild-type, *get1*Δ, *get2*Δ and *atg32*Δ cells expressing mito-DHFR-mCherry and wild-type
669 *FAR9* or *FAR9-TM*^{ER} were grown in glycerol medium (Gly), collected at the indicated time points,
670 and subjected to western blotting. **(E)** The amounts of free mCherry in cells analyzed in **(D)** were
671 quantified in three experiments. The signal intensity value of free mCherry in wild-type cells at
672 the 72 h time point was set to 100%. Data represent the averages of all experiments, with bars

673 indicating standard deviations (n = 3 independent cultures). Data were analyzed by two-tailed
674 Student's t test **(B, C, E)**.
675
676 Figure 6. **Artificial mitochondrial anchoring of the Far complex partially reduces mitophagy.**
677 **(A)** Representative images of wild-type, *get1*Δ, and *get2*Δ cells expressing the endogenous
678 Far9/10 or a variant whose TA domains were replaced with the Gem1 TM domain (*FAR9/FAR10-*
679 *TM*^{MITO}) grown for 24 h in glycerol medium (Gly) and observed by structured illumination
680 microscopy. All strains were derivatives expressing mito-DHFR-mCherry and Far8-3×GFP. Scale
681 bar, 2 μm. **(B)** Cells analyzed in **(A)** were quantified in three experiments. Data represent the
682 averages of all experiments, with bars indicating standard deviations (n = 3 independent cultures).
683 **(C)** Wild-type, *get1*Δ, *get2*Δ, and *atg32*Δ cells expressing mito-DHFR-mCherry and the
684 endogenous Far9/10 or Far9/Far10-TA^{MITO} were grown in glycerol medium (Gly), collected at the
685 indicated time points, and subjected to western blotting. **(D)** The amounts of free mCherry in cells
686 analyzed in **(C)** were quantified in three experiments. The signal intensity value of free mCherry
687 in wild-type cells at the 72 h time point was set to 100%. Data represent the averages of all
688 experiments, with bars indicating standard deviations (n = 3 independent cultures). Data were
689 analyzed by one-way ANOVA with Dunnett's multiple comparison test **(B, D)**.
690
691 Figure 7. **Msp1 is required for efficient mitophagy in cells lacking Get3. (A)** Wild-type, *msp1*Δ,
692 *get3*Δ, *msp1*Δ *get3*Δ, the endogenous *MSP1*-expressing or *MSP1 E193Q* (*MSP1EQ*)-expressing
693 *get3*Δ, and *atg32*Δ cells were grown in glycerol medium (Gly), collected at the indicated time
694 points, and subjected to western blotting. All strains were derivatives expressing mito-DHFR-
695 mCherry. **(B)** The amount of free mCherry in cells analyzed in **(A)** was quantified in three
696 experiments. The signal intensity value of free mCherry in wild-type cells at the 72 h time point

was set to 100%. Data represent the averages of all experiments, with bars indicating standard deviations (n = 3 independent cultures). **(C)** Representative images of wild-type, *msp1*Δ, *get3*Δ, and *msp1*Δ *get3*Δ cells expressing mito-DHFR-mCherry and Far8-3×GFP grown for 24 h in glycerol medium (Gly) and observed by structured illumination microscopy. Scale bar, 2 μm. **(D)** Cells analyzed in **(C)** were quantified in three experiments. Data represent the averages of all experiments, with bars indicating standard deviations (n = 3 independent cultures). **(E)** Wild-type, *ppg1*Δ, *msp1*Δ, *get3*Δ, *msp1*Δ *ppg1*Δ, *get3*Δ *ppg1*Δ, *msp1*Δ *get3*Δ, *msp1*Δ *get3*Δ *ppg1*Δ, and *atg32*Δ cells expressing mito-DHFR-mCherry were grown in glycerol medium (Gly), collected at the indicated time points, and subjected to western blotting. **(F)** The amount of free mCherry in cells analyzed in **(E)** was quantified in three experiments. The signal intensity value of free mCherry in wild-type cells at the 72 h time point was set to 100%. Data represent the averages of all experiments, with bars indicating standard deviations (n = 3 independent cultures). Data were analyzed by one-way ANOVA with Dunnett's multiple comparison test **(B)**, or two-tailed Student's t test **(F)**.

Figure 8. **A hypothetical model for activation of Atg32-mediated mitophagy. (Upper panel)** Under mitophagy-noninducing (fermentable) conditions, a substantial fraction of the Ppg1-Far complex escapes the GET pathway that may have reduced levels, activity, and/or affinity, localizes to mitochondria, and suppress Atg32 phosphorylation and Atg32-Atg11 interactions. Mitochondria-anchored Ppg1-Far can be extracted from the OMM via Msp1. **(Lower panel)** Under mitophagy-inducing (non-fermentable) conditions, the GET pathway efficiently mediates targeting of the Ppg1-Far complex to the ER, which in turn promotes Atg32 phosphorylation and Atg32-Atg11 interactions. Msp1-dependent extraction of mitochondria-anchored Ppg1-Far from the OMM may be enhanced by unknown mechanisms, contributing to activation of mitophagy.

Figure legends

Figure S1. **Expression of a catalytically inactive Ppg1 mutant restores Atg32-Atg11 interactions and mitophagy in *get1/2*-null cells. (A)** A schematic illustration of the NanoBiT system using cells expressing Atg32-3HA-3×GFP-3FLAG-LgBiT and Atg11-HA-SmBiT. Upon mitophagy induction, Atg32 interacts with Atg11, bringing each luminescent subunit into close proximity to form a functional unit that releases a luminescent signal, which is detected by a microplate reader. **(B)** Derivatives of cells analyzed in **(C)** expressing Atg32-3HA-3×GFP-3FLAG-LgBiT and Atg11-HA-SmBiT, or wild-type cells expressing Atg32 and Atg11 (negative control, N.C.), were grown in glycerol medium (Gly), collected at the OD_{600} = 1.4 point, incubated with substrates, and subjected to the NanoBiT-based bioluminescence assay. Data represent the averages of all experiments, with bars indicating standard deviations (n = 3 independent cultures). **(C)** Wild-type, *get1*Δ, and *get2*Δ cells containing chromosomally integrated wild-type *PPG1* or *PPG1 H111N* were grown in glycerol medium (Gly), collected at the indicated time points, and subjected to western blotting. **(D)** The amounts of free mCherry in cells analyzed in **(C)** was quantified in three experiments. The signal intensity value of free mCherry in wild-type cells at the 72 h time point was set to 100%. Data represent the averages of all experiments, with bars indicating standard deviations (n = 3 independent cultures). Data were analyzed by two-tailed Student's t test **(B, D)**.

Figure S2. **ER localization of the Far complex is perturbed in GET-deficient cells. (A)** Representative images of wild-type, *get2*Δ, and *get3*Δ cells expressing mito-DHFR-mCherry and Far8-3×GFP grown for 24 h in glycerol medium (Gly) and observed by structured illumination microscopy. Scale bar, 2 μm. The percentage of cells exhibiting mitochondria-localized Far8-3×GFP is depicted. **(B)** Representative images of wild-type cells expressing the endogenous

GET1/2, chromosomally integrated *GET1 NRm (N72A, R73A*), or a *GET2 RERRm (R14E, E15R, R16E, R17E*) grown for 24 h in glycerol medium (Gly) and observed by structured illumination microscopy. All strains were derivatives expressing mito-DHFR-mCherry and Far8-3×GFP. Scale bar, 2 μm. The percentage of cells exhibiting mitochondria-localized Far8-3×GFP is depicted. **(C)** Wild-type, *get1*Δ, *get2*Δ, or cells expressing chromosomally integrated *GET1 NRm* or *GET2 RERRm,* and *atg32*Δ cells were grown in glycerol medium (Gly), collected at the indicated time points, and subjected to western blotting. **(D)** The amounts of free mCherry in cells analyzed in **(C)** was quantified in three experiments. The signal intensity value of free mCherry in wild-type cells at the 72 h time point was set to 100%. Data represent the averages of all experiments, with bars indicating standard deviations (n = 3 independent cultures). **(E)** Wild-type, *atg32*Δ, *atg39*Δ *atg40*Δ, and *atg32*Δ *atg39*Δ *atg40*Δ cells expressing mito-DHFR-mCherry and Far8-3×GFP were grown in glycerol medium (Gly), collected at the indicated time points, and subjected to western blotting. Generation of free GFP indicates transport of Far8 to the vacuole. **(F)** The amount of free GFP in cells analyzed in **(E)** was quantified in three experiments. The signal intensity value of free GFP in wild-type cells at the 72 h time point was set to 100%. Data represent the averages of all experiments, with bars indicating standard deviations (n = 3 independent cultures). Data were analyzed by one-way ANOVA with Dunnett's multiple comparison test **(D)** or Tukey's multiple comparison test **(F)**.

Figure S3. **Loss of Far10 significantly ameliorates mitophagic deficiencies in the absence of Get1/2. (A)** Wild-type, *far10*Δ, *get1*Δ, *get2*Δ, *get1*Δ *far10*Δ, and *get2*Δ *far10*Δ cells expressing Atg32-3HA-3×GFP-3FLAG-LgBiT and Atg11-HA-SmBiT, or wild-type cells expressing Atg32 and Atg11 (negative control, N.C.) were grown in glycerol medium (Gly), collected at the OD_{600} = 1.4 point, incubated with substrates, and subjected to the NanoBiT-based bioluminescence assay.

Data represent the averages of all experiments, with bars indicating standard deviations (n = 3 independent cultures). **(B)** Wild-type, *far10*Δ, *get1*Δ, *get2*Δ, *get1*Δ *far10*Δ, *get2*Δ *far10*Δ, and *atg32*Δ cells expressing mito-DHFR-mCherry were grown in glycerol medium (Gly), collected at the indicated time points, and subjected to western blotting. **(C)** The amount of free mCherry in cells analyzed in **(B)** was quantified in six experiments. The signal intensity value of free mCherry in wild-type cells at the 72 h time point was set to 100%. Data represent the averages of all experiments, with bars indicating standard deviations (n = 6 independent cultures). Data were analyzed by two-tailed Student's t test **(A, C)**.

Figure S4. **Artificial ER anchoring of the Far complex in *get1/2*-null cells. (A)** Representative images of wild-type, *get1*Δ, and *get2*Δ cells expressing the endogenous Far9 or a variant whose TA domain was replaced with the Sec12 TM domain (*FAR9-TM*^{ER}) grown for 24 h in glycerol medium (Gly) and observed by structured illumination microscopy. All strains were derivatives expressing mito-DHFR-mCherry and Far8-3×GFP. Scale bar, 2 μm. **(B)** Cells analyzed in **(A)** were quantified in three experiments. Data represent the averages of all experiments, with bars indicating standard deviations. Data were analyzed by two-tailed Student's t test **(B)**.

Figure S5. **Suppression of mitophagy by artificially mitochondria-anchored Ppg1-Far and restoration of mitophagy in *get3/msp1*-double-null cells expressing a Atg32 variant defective in Ppg1-Far interaction. (A)** Wild-type cells expressing the endogenous *FAR9* and *PPG1* or chromosomally integrated *FAR9/FAR10-TA*^{MITO} and *PPG1 H111N* were grown in glycerol medium (Gly), collected at the indicated time points, and subjected to western blotting. **(B)** The amounts of free mCherry in cells analyzed in **(A)** were quantified in three experiments. The signal intensity value of free mCherry in wild-type cells at the 72 h time point was set to 100%. Data

represent the averages of all experiments, with bars indicating standard deviations (n = 3 independent cultures). Data were analyzed by two-tailed Student's t test **(B)**. **(C)** Wild-type, *msp1*Δ, *get3*Δ, and *msp1*Δ *get3*Δ cells expressing the endogenous *ATG32* or chromosomally integrated *ATG32(Δ151-200)* were grown in glycerol medium (Gly), collected at the indicated time points, and subjected to western blotting. **(D)** The amounts of free mCherry in cells analyzed in **(C)** were quantified in three experiments. The signal intensity value of free mCherry in wild-type cells at the 72 h time point was set to 100%. Data represent the averages of all experiments, with bars indicating standard deviations (n = 3 independent cultures). Data were analyzed by two-tailed Student's t test **(B and D)**.

Table S1. Yeast strains used in this study

Strain name	Genotype	Source
BY4741	*his3Δ1 leu2Δ0 met15Δ0 ura3Δ0*	(1)
KOY1387	BY4741 *TEF^{P}-mito-DHFR-mCherry::CgHIS3*	
KOY1422	BY4741 *TEF^{P}-mito-DHFR-mCherry::CgHIS3 atg32::kanMX6*	
KOY2928	BY4741 *TEF^{P}-mito-DHFR-mCherry::CgHIS3 get2::natNT2*	
KOY4146	BY4741 *TEF^{P}-mito-DHFR-mCherry::CgHIS3 get1::natNT2*	
KOY4594	BY4741 *TEF^{P}-mito-DHFR-mCherry::CgHIS3 atg32::KlURA3 atg32::ATG32-3HA*	
KOY4860	BY4741 *TEF^{P}-mito-DHFR-mCherry::CgHIS3 msp1::natNT2*	
KOY5408	BY4741 *pep4::kanMX6 prb1::hphNT1 atg32::zeoNT3*	
KOY5558	BY4741 *pep4::kanMX6 prb1::hphNT1 atg32::zeoNT3 get1::natNT2* [pRS316-*ATG32-3HA*]	
KOY5560	BY4741 *pep4::kanMX6 prb1::hphNT1 atg32::zeoNT3 get2::natNT2* [pRS316-*ATG32-3HA*]	
KOY5562	BY4741 *pep4::kanMX6 prb1::hphNT1 atg32::zeoNT3 get3::natNT2* [pRS316-*ATG32-3HA*]	
KOY6288	BY4741 *TEF^{P}-mito-DHFR-mCherry::CgHIS3 get3::natNT2 msp1::KlURA3*	
KOY6872	BY4741 *TEF^{P}-mito-DHFR-mCherry::CgHIS3 ppg1::hphNT1*	
KOY6875	BY4741 *TEF^{P}-mito-DHFR-mCherry::CgHIS3 get1::natNT2 ppg1::hphNT1*	
KOY6878	BY4741 *TEF^{P}-mito-DHFR-mCherry::CgHIS3 get2::natNT2 ppg1::hphNT1*	
KOY6996	BY4741 *TEF^{P}-mito-DHFR-mCherry::CgHIS3 atg32::KlURA3 ATG11-HA-SmBiT::hphNT1 ATG32-3HA-3×mGFP-3FLAG-LgBiTn*	
KOY7491	BY4741 *TEF^{P}-mito-DHFR-mCherry::CgHIS3 atg32::KlURA3 ATG11-HA-SmBiT::hphNT1 ATG32-3HA-3×mGFP-3FLAG-LgBiTn get1::natNT2*	
KOY7494	BY4741 *TEF^{P}-mito-DHFR-mCherry::CgHIS3 atg32::KlURA3 ATG11-HA-SmBiT::hphNT1 ATG32-3HA-3×mGFP-3FLAG-LgBiTn get2::natNT2*	
KOY7497	BY4741 *TEF^{P}-mito-DHFR-mCherry::CgHIS3 atg32::KlURA3 ATG11-HA-SmBiT::hphNT1 ATG32-3HA-3×mGFP-3FLAG-LgBiTn ppg1::natNT2*	
KOY7619	BY4741 *TEF^{P}-mito-DHFR-mCherry::CgHIS3 atg32::KlURA3 ATG11-HA-SmBiT::hphNT1 ATG32-3HA-3×mGFP-3FLAG-LgBiTn get1::natNT2 ppg1::kanMX6*	
KOY7622	BY4741 *TEF^{P}-mito-DHFR-mCherry::CgHIS3 atg32::KlURA3 ATG11-HA-SmBiT::hphNT1 ATG32-3HA-3×mGFP-3FLAG-LgBiTn get2::natNT2 ppg1::kanMX6*	

KOY7629	BY4741 *TEF^{P}-mito-DHFR-mCherry::CgHIS3 far9::hphNT1*	
KOY7632	BY4741 *TEF^{P}-mito-DHFR-mCherry::CgHIS3 get1::natNT2 far9::hphNT1*	
KOY7635	BY4741 *TEF^{P}-mito-DHFR-mCherry::CgHIS3 get2::natNT2 far9::hphNT1*	
KOY7794	BY4741 *TEF^{P}-mito-DHFR-mCherry::CgHIS3 atg32::KlURA3 ATG11-HA-SmBiT::hphNT1 ATG32-3HA-3×mGFP-3FLAG-LgBiTn far9::KlURA3*	
KOY7797	BY4741 *TEF^{P}-mito-DHFR-mCherry::CgHIS3 atg32::KlURA3 ATG11-HA-SmBiT::hphNT1 ATG32-3HA-3×mGFP-3FLAG-LgBiTn get1::natNT2 far9::KlURA3*	
KOY7805	BY4741 *TEF^{P}-mito-DHFR-mCherry::CgHIS3 FAR8-3×GFP::hphNT1*	
KOY7807	BY4741 *TEF^{P}-mito-DHFR-mCherry::CgHIS3 get1::natNT2 FAR8-3×GFP::hphNT1*	
KOY7809	BY4741 *TEF^{P}-mito-DHFR-mCherry::CgHIS3 get2::natNT2 FAR8-3×GFP::hphNT1*	
KOY7816	BY4741 *TEF^{P}-mito-DHFR-mCherry::CgHIS3 atg32::KlURA3 ATG11-HA-SmBiT::hphNT1 ATG32-3HA-3×mGFP-3FLAG-LgBiTn get3::natNT2*	
KOY7821	BY4741 *SEC63-mCherry::KlURA3 FAR8-3×GFP::hphNT1*	
KOY7823	BY4741 *SEC63-mCherry::KlURA3 get1::natNT2 FAR8-3×GFP::hphNT1*	
KOY7825	BY4741 *SEC63-mCherry::KlURA3 get2::natNT2 FAR8-3×GFP::hphNT1*	
KOY7853	BY4741 *TEF^{P}-mito-DHFR-mCherry::CgHIS3 FAR8-3×GFP::hphNT1 atg32::natNT2*	
KOY7862	BY4741 *TEF^{P}-mito-DHFR-mCherry::CgHIS3 get1::KlURA3 GET1 FAR8-3×GFP::hphNT1*	
KOY7864	BY4741 *TEF^{P}-mito-DHFR-mCherry::CgHIS3 get1::KlURA3 GET1(N72A, R73A) FAR8-3×GFP::hphNT1*	
KOY7866	BY4741 *TEF^{P}-mito-DHFR-mCherry::CgHIS3 get2::KlURA3 GET2 FAR8-3×GFP::hphNT1*	
KOY7884	BY4741 *TEF^{P}-mito-DHFR-mCherry::CgHIS3 get2::KlURA3 GET2(R14E, E15R, R16E, R17E) FAR8-3×GFP::hphNT1*	
KOY7905	BY4741 *TEF^{P}-mito-DHFR-mCherry::CgHIS3 ppg1::KlURA3 PPG1*	
KOY7907	BY4741 *TEF^{P}-mito-DHFR-mCherry::CgHIS3 ppg1::KlURA3 PPG1(H111N)*	
KOY7973	BY4741 *TEF^{P}-mito-DHFR-mCherry::CgHIS3 ppg1::KlURA3 PPG1 get1::natNT2*	
KOY7976	BY4741 *TEF^{P}-mito-DHFR-mCherry::CgHIS3 ppg1::KlURA3 PPG1(H111N) get1::natNT2*	

KOY7979	BY4741 *TEF^{P}-mito-DHFR-mCherry::CgHIS3 ppg1::KlURA3 PPG1 get2::natNT2*	
KOY7982	BY4741 *TEF^{P}-mito-DHFR-mCherry::CgHIS3 ppg1::KlURA3 PPG1(H111N) get2::natNT2*	
KOY8036	BY4741 *TEF^{P}-mito-DHFR-mCherry::CgHIS3 FAR8-3×GFP::natNT2 far10::kanMX6*	
KOY8039	BY4741 *TEF^{P}-mito-DHFR-mCherry::CgHIS3 get1::natNT2 FAR8-3×GFP::hphNT1 far10::kanMX6*	
KOY8045	BY4741 *TEF^{P}-mito-DHFR-mCherry::CgHIS3 atg32::KlURA3 atg32(Δ151-200)-3HA*	
KOY8046	BY4741 *TEF^{P}-mito-DHFR-mCherry::CgHIS3 get1::natNT2 atg32::KlURA3 ATG32-3HA*	
KOY8047	BY4741 *TEF^{P}-mito-DHFR-mCherry::CgHIS3 get1::natNT2 atg32::KlURA3 atg32(Δ151-200)-3HA*	
KOY8049	BY4741 *TEF^{P}-mito-DHFR-mCherry::CgHIS3 get2::natNT2 atg32::KlURA3 ATG32-3HA*	
KOY8050	BY4741 *TEF^{P}-mito-DHFR-mCherry::CgHIS3 get2::natNT2 atg32::KlURA3 atg32(Δ151-200)-3HA*	
KOY8051	BY4741 *TEF^{P}-mito-DHFR-mCherry::CgHIS3 FAR8-3×GFP::natNT2 far9::KlURA3*	
KOY8054	BY4741 *TEF^{P}-mito-DHFR-mCherry::CgHIS3 get1::natNT2 FAR8-3×GFP::hphNT1 far9::KlURA3*	
KOY8066	BY4741 *TEF^{P}-mito-DHFR-mCherry::CgHIS3 far10::KlURA3*	
KOY8069	BY4741 *TEF^{P}-mito-DHFR-mCherry::CgHIS3 get1::natNT2 far10::natNT2*	
KOY8072	BY4741 *TEF^{P}-mito-DHFR-mCherry::CgHIS3 get2::natNT2 far10::natNT2*	
KOY8075	BY4741 *TEF^{P}-mito-DHFR-mCherry::CgHIS3 atg32::KlURA3 ATG11-HA-SmBiT::hphNT1 ATG32-3HA-3×mGFP-3FLAG-LgBiTn ppg1::KlURA3 PPG1*	
KOY8076	BY4741 *TEF^{P}-mito-DHFR-mCherry::CgHIS3 atg32::KlURA3 ATG11-HA-SmBiT::hphNT1 ATG32-3HA-3×mGFP-3FLAG-LgBiTn ppg1::KlURA3 PPG1(H111N)*	
KOY8077	BY4741 *TEF^{P}-mito-DHFR-mCherry::CgHIS3 FAR8-3×GFP::kanMX6*	
KOY8079	BY4741 *TEF^{P}-mito-DHFR-mCherry::CgHIS3 get1::natNT2 FAR8-3×GFP::kanMX6*	
KOY8081	BY4741 *TEF^{P}-mito-DHFR-mCherry::CgHIS3 get2::natNT2 FAR8-*	

	3×GFP::kanMX6	
KOY8092	BY4741 *TEF^{P}-mito-DHFR-mCherry::CgHIS3 atg32::KlURA3 ATG11-HA-SmBiT::hphNT1 ATG32-3HA-3×mGFP-3FLAG-LgBiTn ppg1::KlURA3 PPG1 get1::natNT2*	
KOY8095	BY4741 *TEF^{P}-mito-DHFR-mCherry::CgHIS3 atg32::KlURA3 ATG11-HA-SmBiT::hphNT1 ATG32-3HA-3×mGFP-3FLAG-LgBiTn ppg1::KlURA3 PPG1 get2::natNT2*	
KOY8098	BY4741 *TEF^{P}-mito-DHFR-mCherry::CgHIS3 atg32::KlURA3 ATG11-HA-SmBiT::hphNT1 ATG32-3HA-3×mGFP-3FLAG-LgBiTn ppg1::KlURA3 PPG1(H111N) get1::natNT2*	
KOY8101	BY4741 *TEF^{P}-mito-DHFR-mCherry::CgHIS3 atg32::KlURA3 ATG11-HA-SmBiT::hphNT1 ATG32-3HA-3×mGFP-3FLAG-LgBiTn ppg1::KlURA3 PPG1(H111N) get2::natNT2*	
KOY8107	BY4741 *TEF^{P}-mito-DHFR-mCherry::CgHIS3 atg32::KlURA3 ATG11-HA-SmBiT::hphNT1 ATG32-3HA-3×mGFP-3FLAG-LgBiTn far10::KlURA3*	
KOY8110	BY4741 *TEF^{P}-mito-DHFR-mCherry::CgHIS3 atg32::KlURA3 ATG11-HA-SmBiT::hphNT1 ATG32-3HA-3×mGFP-3FLAG-LgBiTn get1::natNT2 far10::KlURA3*	
KOY8113	BY4741 *TEF^{P}-mito-DHFR-mCherry::CgHIS3 atg32::KlURA3 ATG11-HA-SmBiT::hphNT1 ATG32-3HA-3×mGFP-3FLAG-LgBiTn get2::natNT2 far10::KlURA3*	
KOY8115	BY4741 *TEF^{P}-mito-DHFR-mCherry::CgHIS3 atg32::KlURA3 ATG11-HA-SmBiT::hphNT1 ATG32-3HA-3×mGFP-3FLAG-LgBiTn far9::KlURA3 get2::natNT2*	
KOY8179	BY4741 *TEF^{P}-mito-DHFR-mCherry::CgHIS3 FAR8-3×GFP::hphNT1 FAR9-TM^{ER}::kanMX6*	
KOY8181	BY4741 *TEF^{P}-mito-DHFR-mCherry::CgHIS3 get1::natNT2 FAR8-3×GFP::hphNT1 FAR9-TM^{ER}::kanMX6*	
KOY8183	BY4741 *TEF^{P}-mito-DHFR-mCherry::CgHIS3 get2::natNT2 FAR8-3×GFP::hphNT1 FAR9-TM^{ER}::kanMX6*	
KOY8192	BY4741 *TEF^{P}-mito-DHFR-mCherry::CgHIS3 msp1::KlURA3 MSP1(E193Q)*	
KOY8235	BY4741 *TEF^{P}-mito-DHFR-mCherry::CgHIS3 get3::natNT2 FAR8-3×GFP::kanMX6*	
KOY8347	BY4741 *TEF^{P}-mito-DHFR-mCherry::CgHIS3 atg32::KlURA3 ATG32-3HA msp1::natNT2*	

KOY8350	BY4741 *TEF^{P}-mito-DHFR-mCherry::CgHIS3 atg32::KlURA3 atg32(Δ151-200)-3HA msp1::natNT2*	
KOY8353	BY4741 *TEF^{P}-mito-DHFR-mCherry::CgHIS3 atg32::KlURA3 ATG32-3HA get3::natNT2*	
KOY8356	BY4741 *TEF^{P}-mito-DHFR-mCherry::CgHIS3 atg32::KlURA3 atg32(Δ151-200)-3HA get3::natNT2*	
KOY8386	BY4741 *TEF^{P}-mito-DHFR-mCherry::CgHIS3 msp1::natNT2 ppg1::zeoNT3*	
KOY8389	BY4741 *TEF^{P}-mito-DHFR-mCherry::CgHIS3 get3::natNT2 ppg1::zeoNT3*	
KOY8392	BY4741 *TEF^{P}-mito-DHFR-mCherry::CgHIS3 get3::natNT2 msp1::KlURA3 ppg1::zeoNT3*	
KOY8401	BY4741 *TEF^{P}-mito-DHFR-mCherry::CgHIS3 atg32::KlURA3 ATG32-3HA msp1::natNT2 get3::zeoNT3*	
KOY8404	BY4741 *TEF^{P}-mito-DHFR-mCherry::CgHIS3 atg32::KlURA3 atg32(Δ151-200)-3HA msp1::natNT2 get3::zeoNT3*	
KOY8440	BY4741 *TEF^{P}-mito-DHFR-mCherry::CgHIS3 atg32::KlURA3 ATG11-HA-SmBiT::hphNT1 ATG32-3HA-3×mGFP-3FLAG-LgBiTn FAR9-TM^{ER}::kanMX6*	
KOY8442	BY4741 *TEF^{P}-mito-DHFR-mCherry::CgHIS3 atg32::KlURA3 ATG11-HA-SmBiT::hphNT1 ATG32-3HA-3×mGFP-3FLAG-LgBiTn get1::natNT2 FAR9-TM^{ER}::kanMX6*	
KOY8444	BY4741 *TEF^{P}-mito-DHFR-mCherry::CgHIS3 atg32::KlURA3 ATG11-HA-SmBiT::hphNT1 ATG32-3HA-3×mGFP-3FLAG-LgBiTn get2::natNT2 FAR9-TM^{ER}::kanMX6*	
KOY8446	BY4741 *TEF^{P}-mito-DHFR-mCherry::CgHIS3 msp1::natNT2 FAR8-3×GFP::kanMX6*	
KOY8554	BY4741 *TEF^{P}-mito-DHFR-mCherry::CgHIS3 FAR8-3×GFP::kanMX6 atg39::KlURA3 atg40::zeoNT3*	
KOY8557	BY4741 *TEF^{P}-mito-DHFR-mCherry::CgHIS3 FAR8-3×GFP::hphNT1 atg32::natNT2 atg39::KlURA3 atg40::zeoNT3*	
KOY8568	BY4741 *TEF^{P}-mito-DHFR-mCherry::CgHIS3 FAR8-3×GFP::natNT2 FAR9-TA^{MITO}::hphNT1 FAR10-TA^{MITO}::kanMX6*	
KOY8570	BY4741 *TEF^{P}-mito-DHFR-mCherry::CgHIS3 ppg1::KlURA3 PPG1 FAR8-3×GFP::natNT2 FAR9-TA^{MITO}::hphNT1 FAR10-TA^{MITO}::kanMX6*	
KOY8572	BY4741 *TEF^{P}-mito-DHFR-mCherry::CgHIS3 ppg1::KlURA3 PPG1(H111N) FAR8-3×GFP::natNT2 FAR9-TA^{MITO}::hphNT1 FAR10-TA^{MITO}::kanMX6*	

KOY8719	BY4741 *TEF^{P}-mito-DHFR-mCherry::CgHIS3 msp1::KlURA3 MSP1(E193Q) get3::natNT2*	
KOY8793	BY4741 *SEC63-mCherry::KlURA3 FAR8-3×GFP::hphNT1 FAR9-TM^{ER}::kanMX6*	
KOY8795	BY4741 *SEC63-mCherry::KlURA3 get1::natNT2 FAR8-3×GFP::hphNT1 FAR9-TM^{ER}::kanMX6*	
KOY9095	BY4741 *SEC63-mCherry::KlURA3 get2::natNT2 FAR8-3×GFP::kanMX6 FAR9-TM^{ER}::hphNT1*	

1. Brachmann, C.B., Davies, A., Cost, G.J., Caputo, E., Li, J., Hieter, P. and Boeke, J.D. (1998). Designer deletion strains derived from *Saccharomyces cerevisiae* S288C: a useful set of strains and plasmids for PCR-mediated gene disruption and other applications. *Yeast* **14**, 115-132.

Table S2. Plasmid used in this study

Plasmid number	Name	Relevant characteristics
KOB71	pRS316-*ATG32-3HAn*	*CEN URA3 580 bp 5′-UTR & 744 bp 3′-UTR from ATG32*

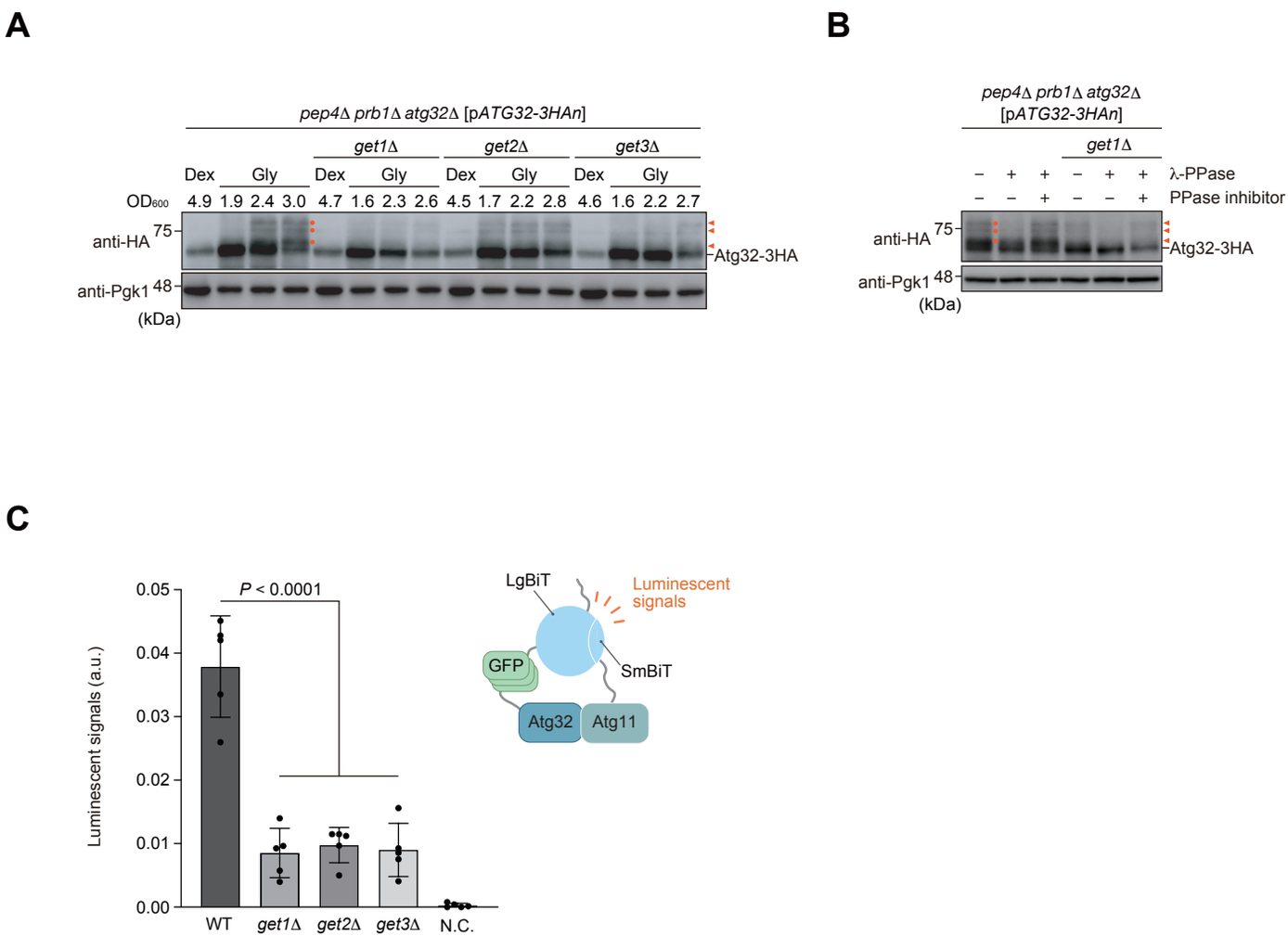

A

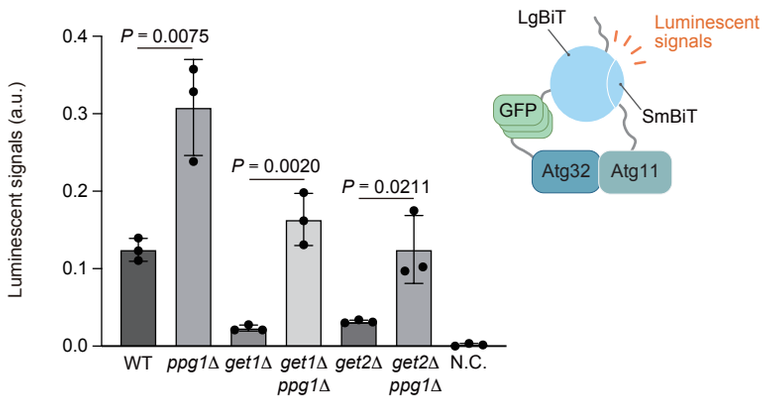

B

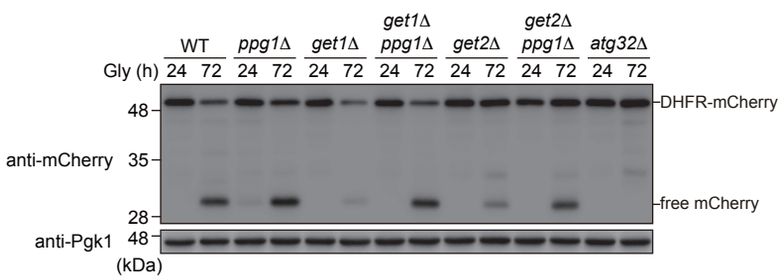

C

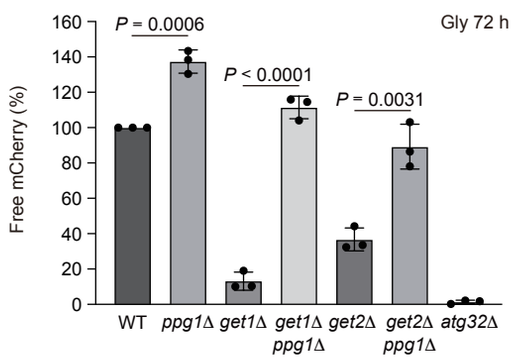

D

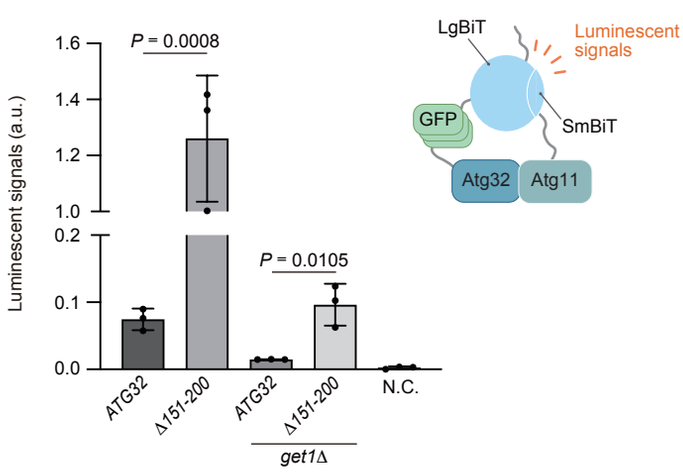

E

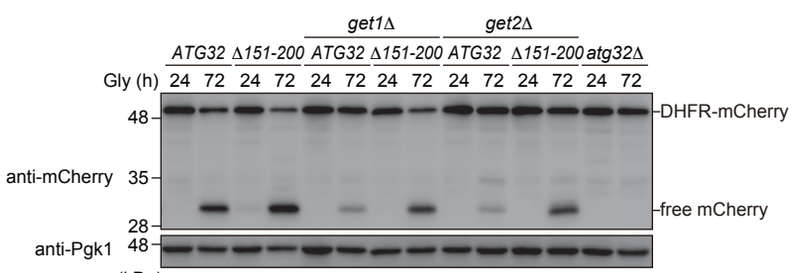

F

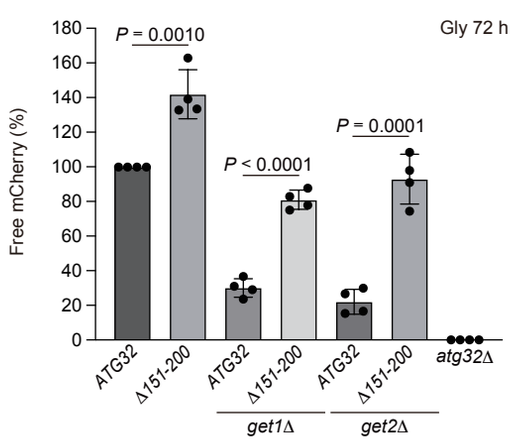

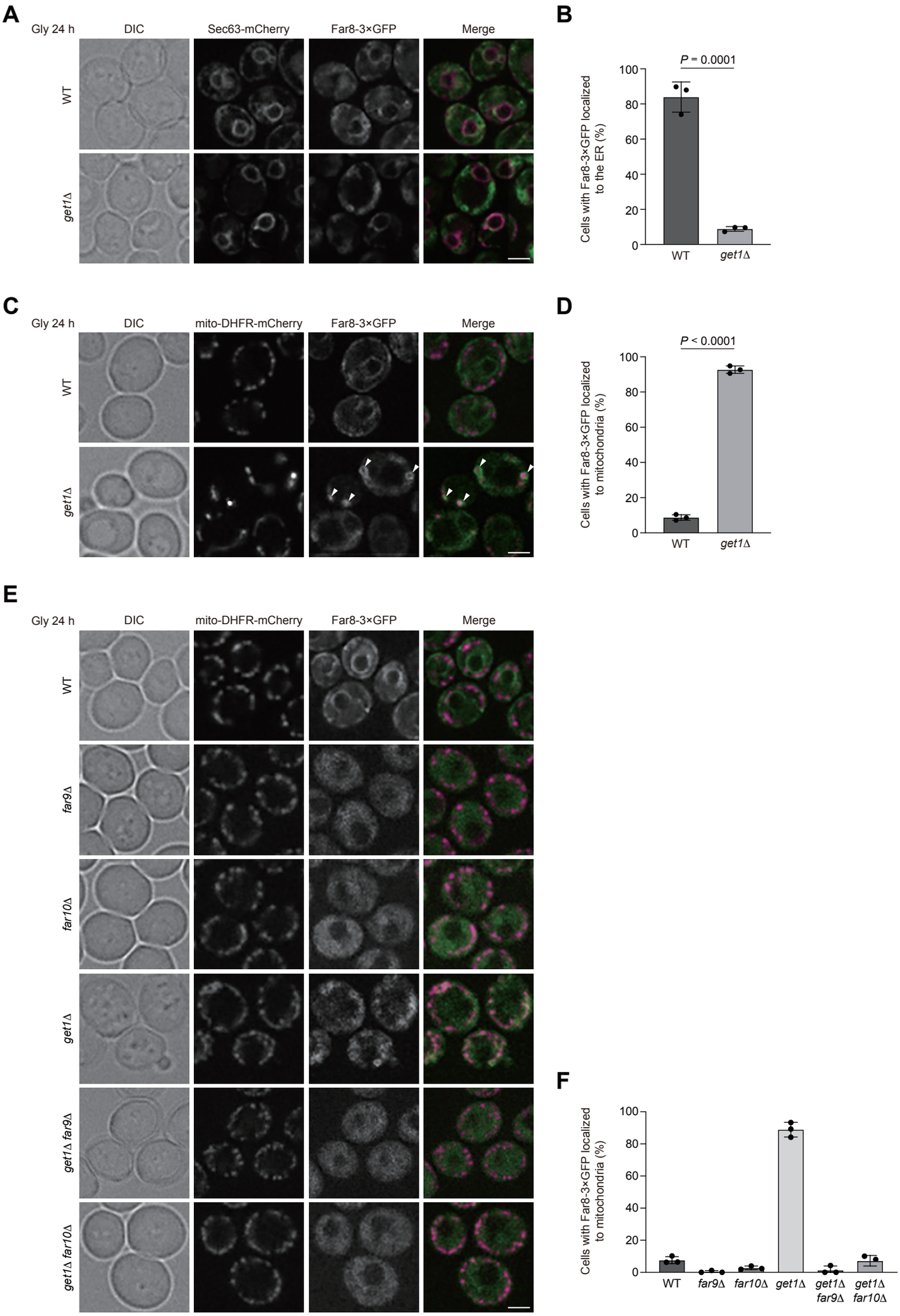

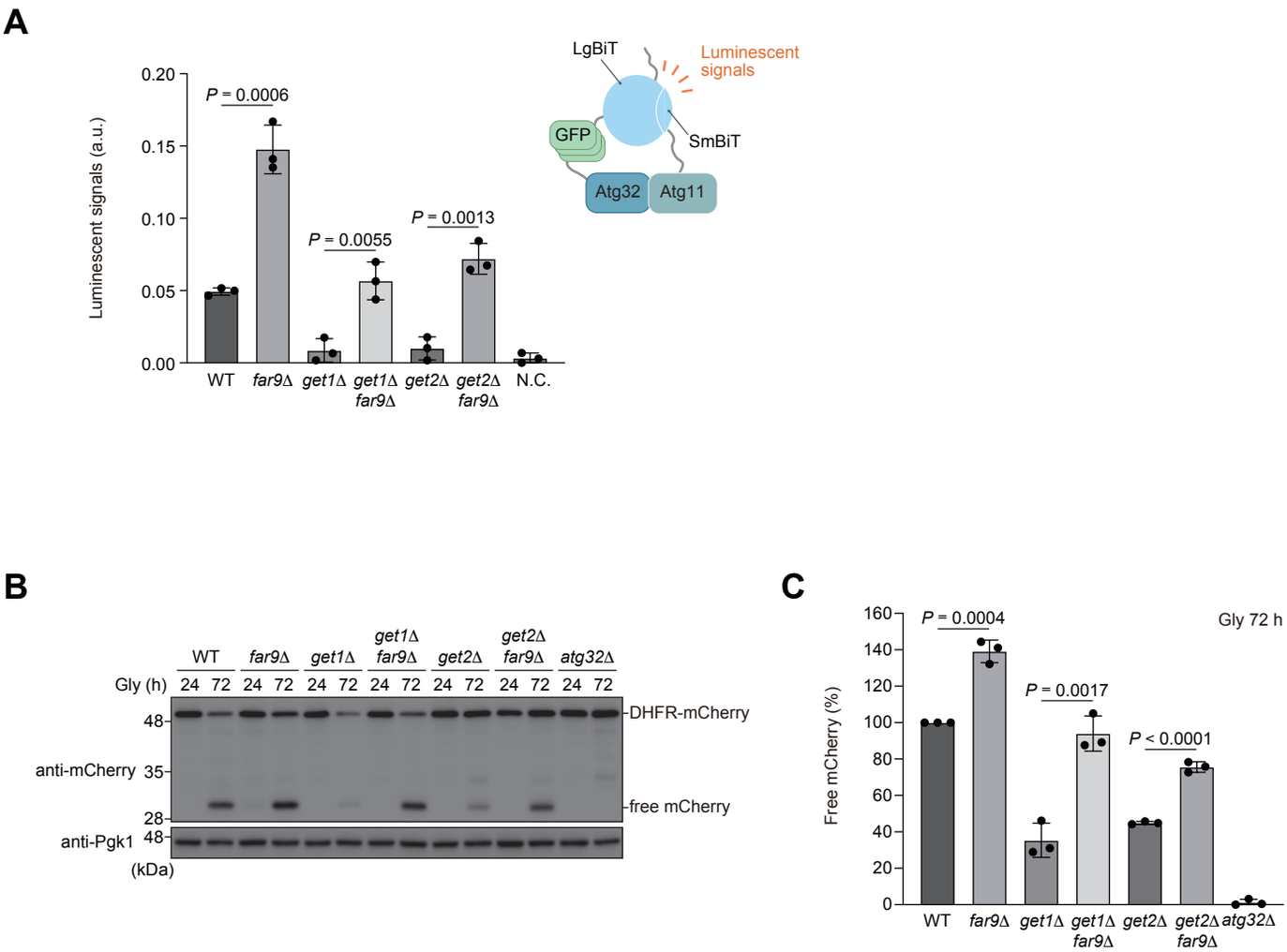

A

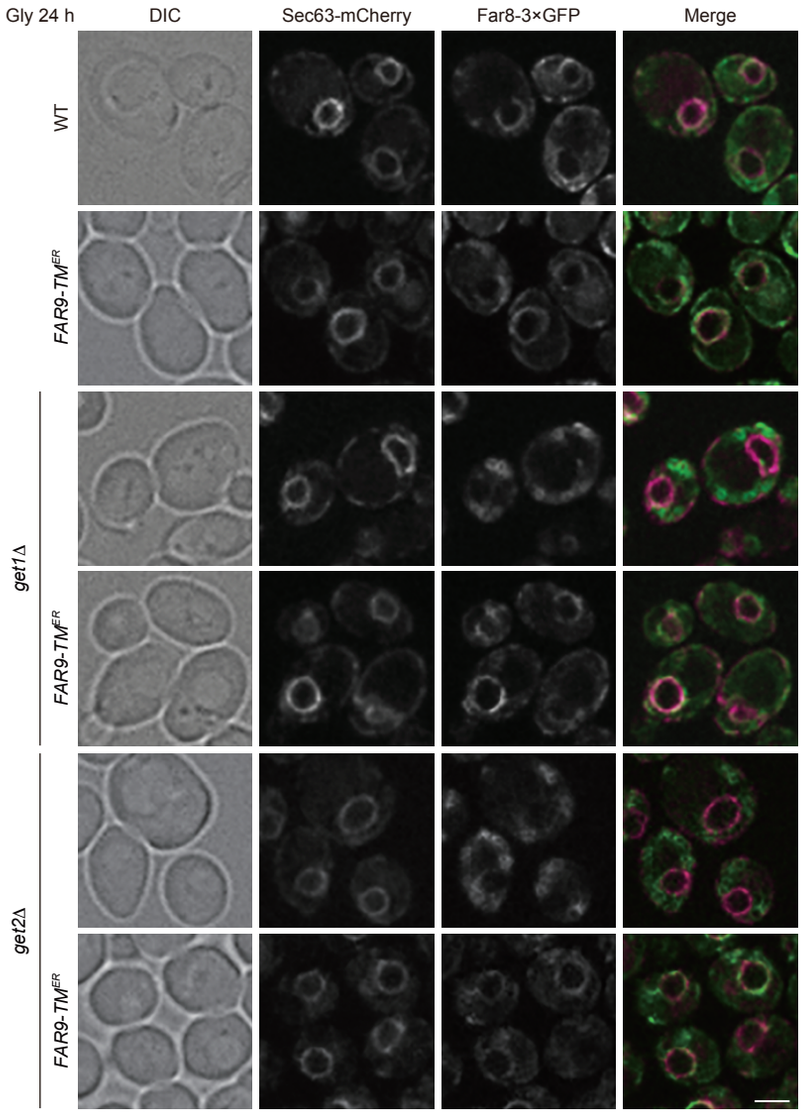

B

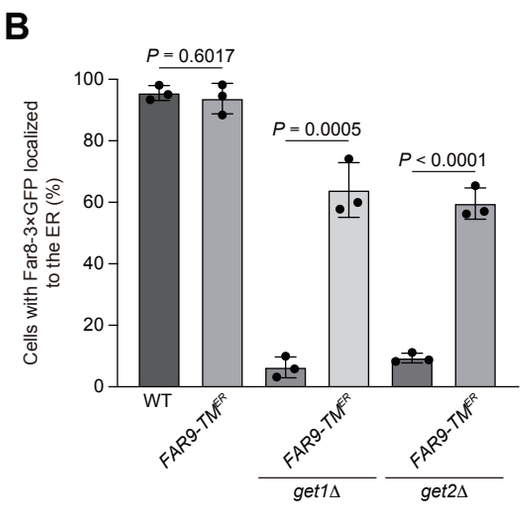

C

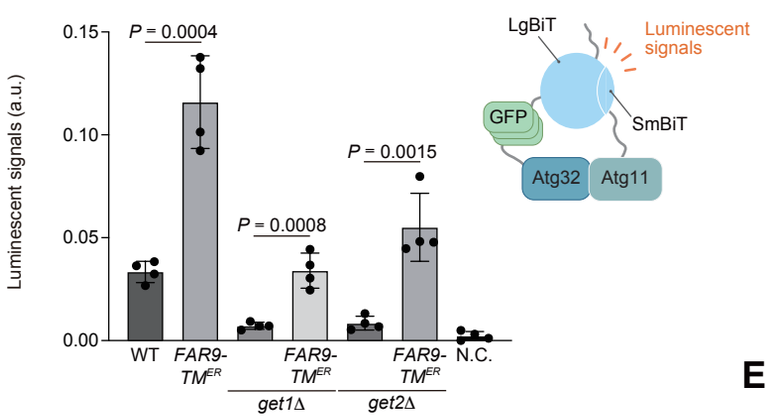

D

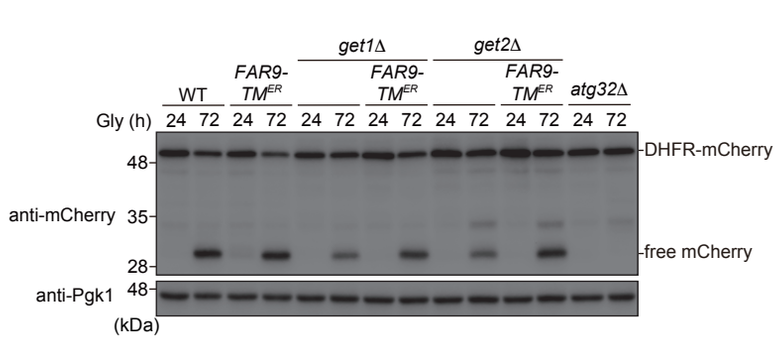

E

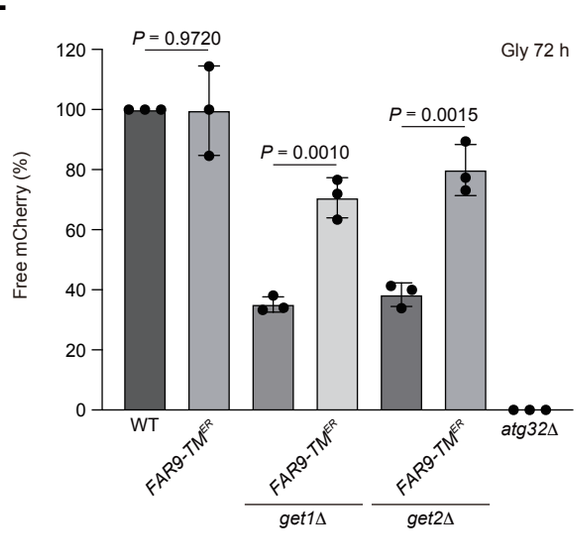

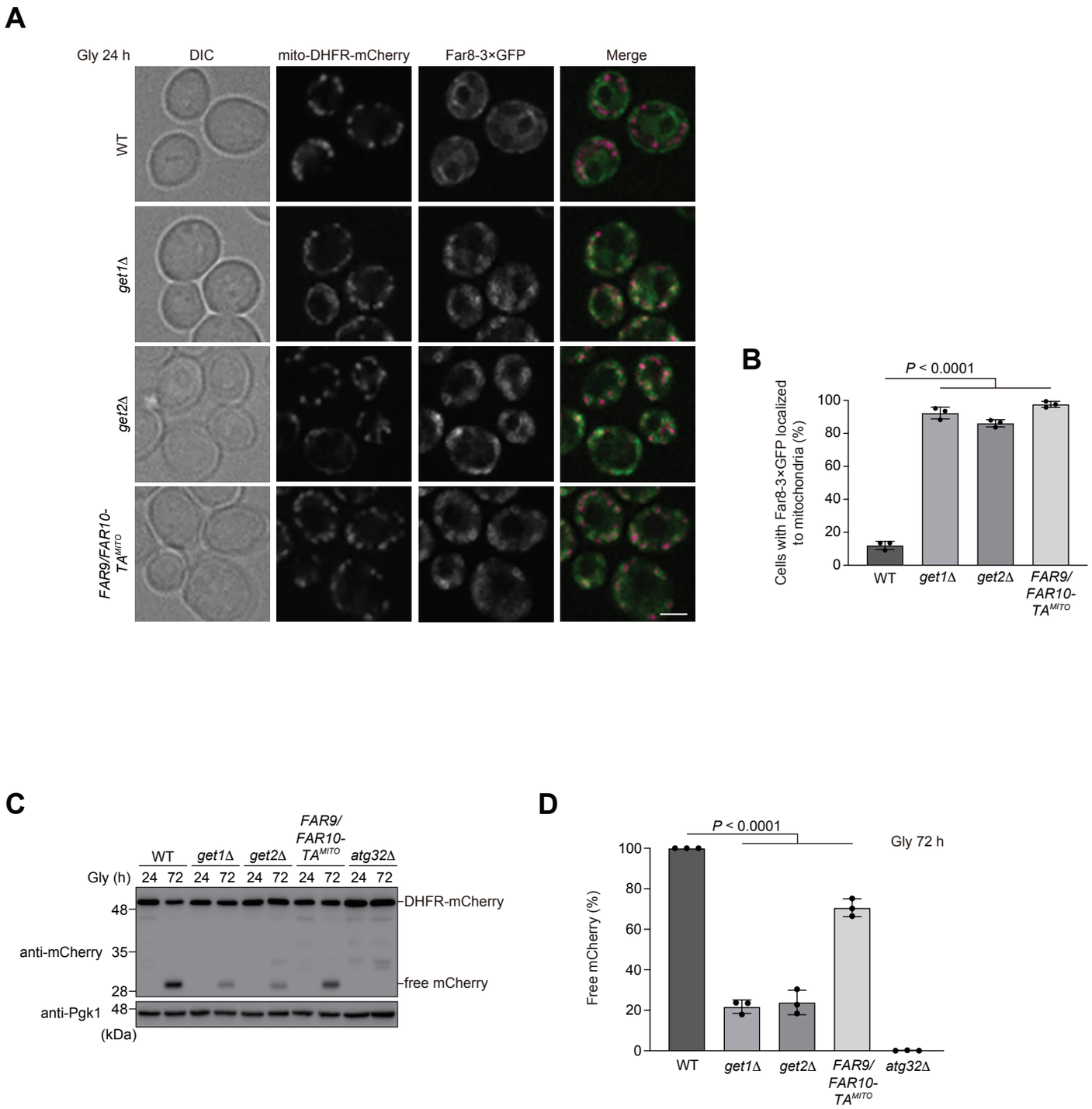

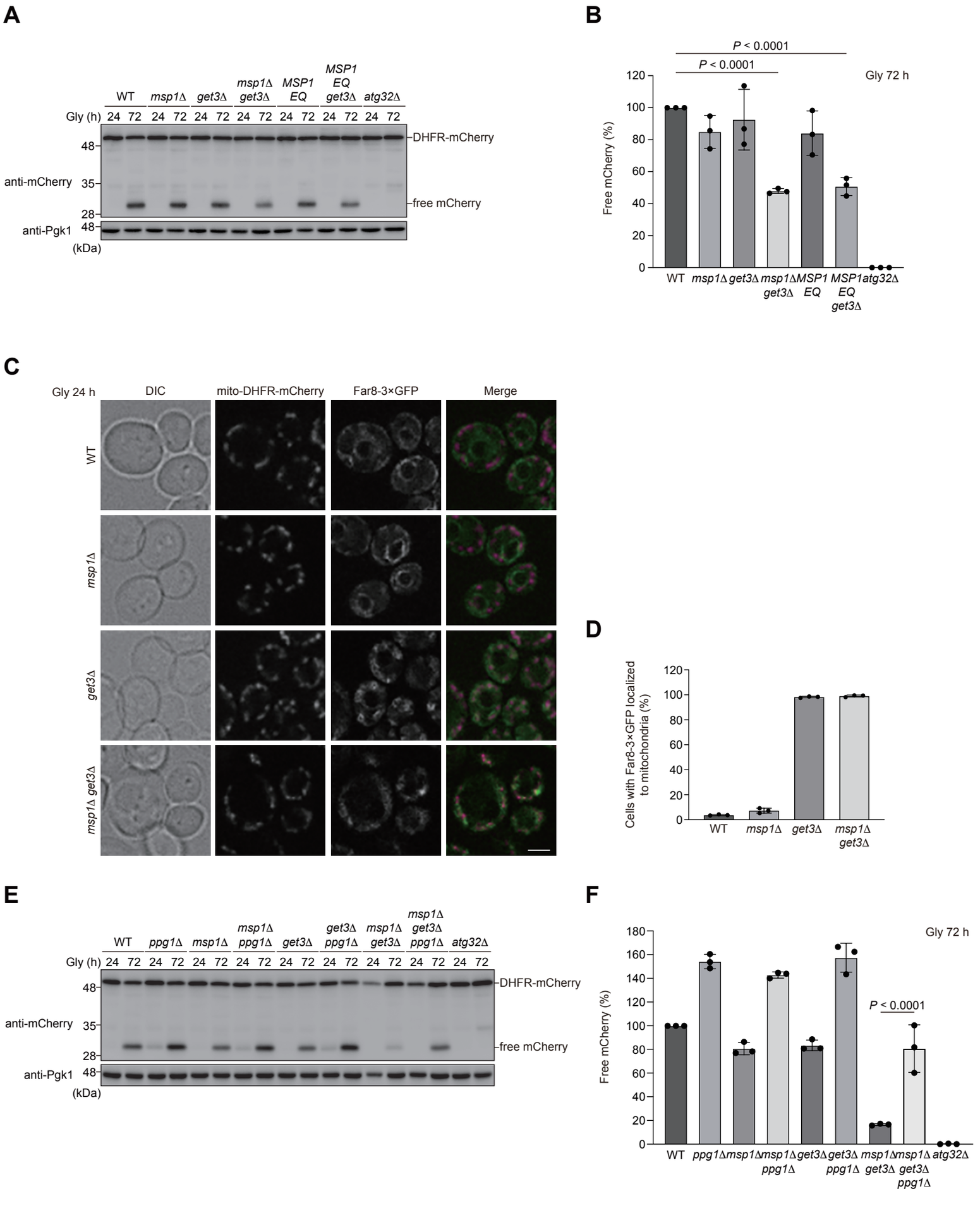

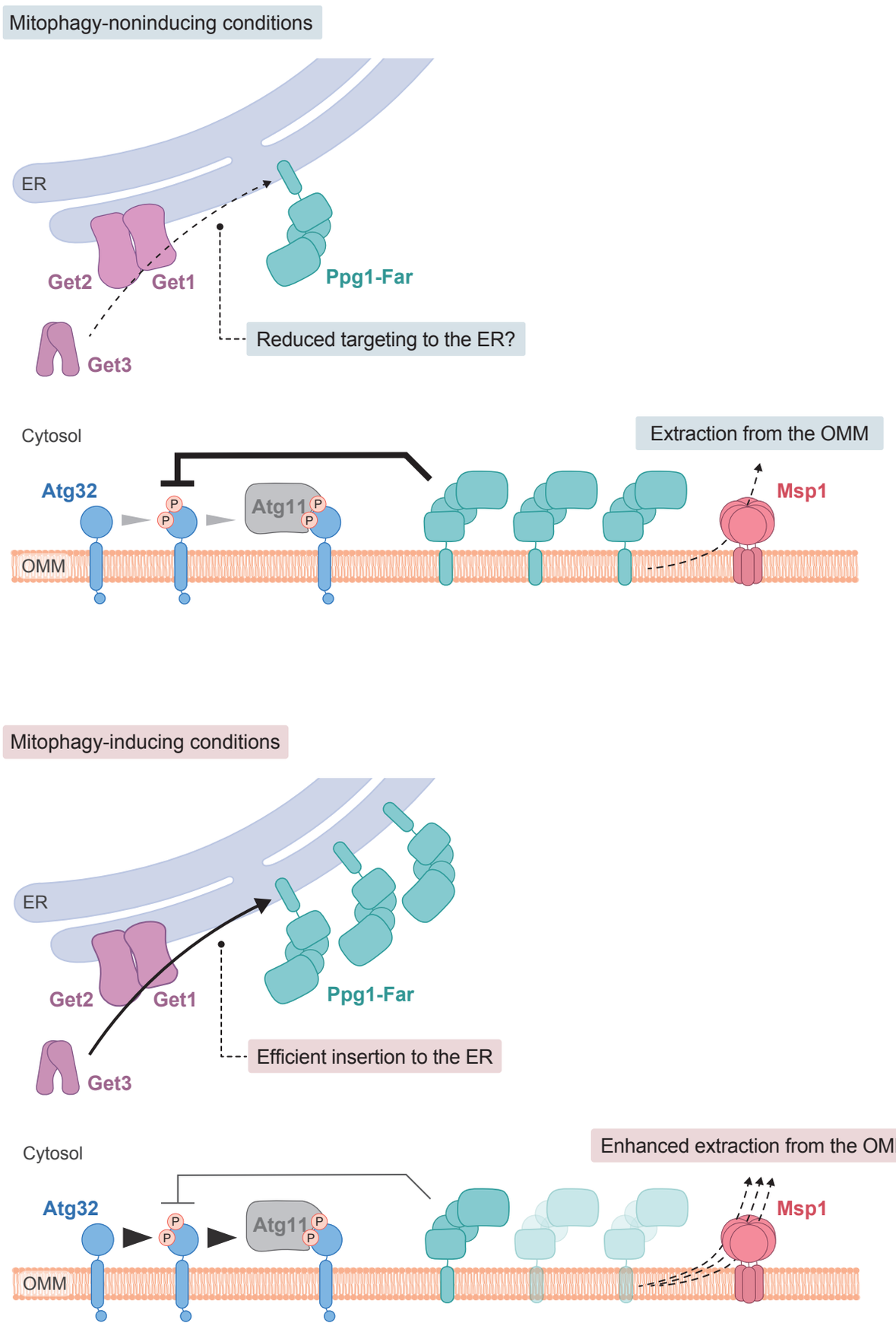

A

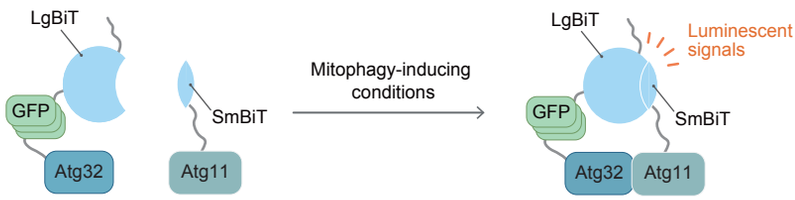

B

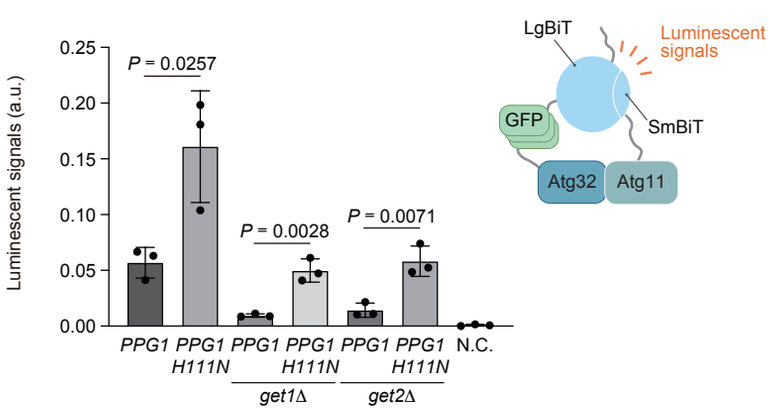

C

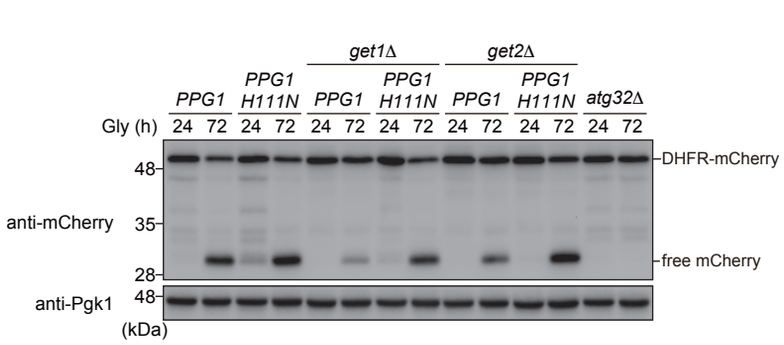

D

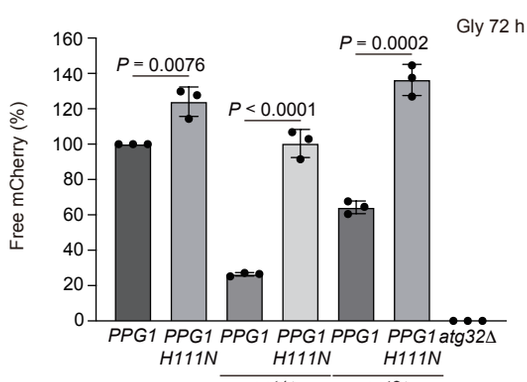

A

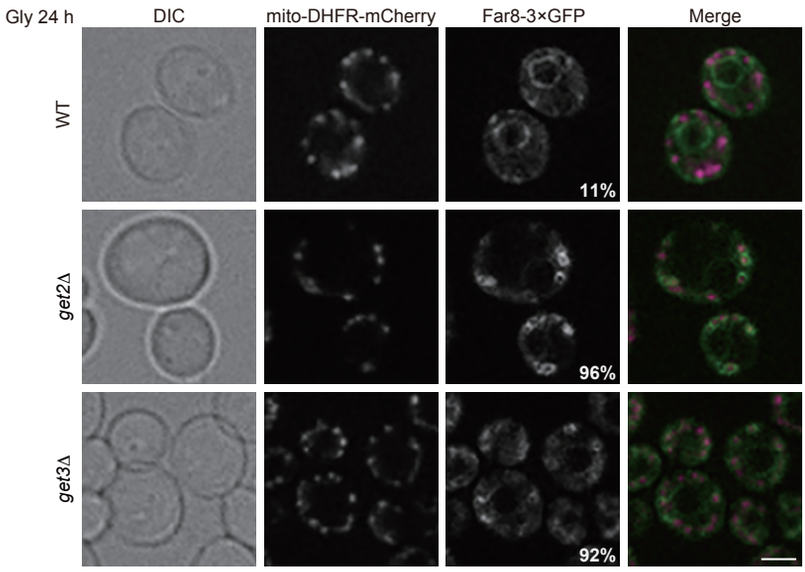

B

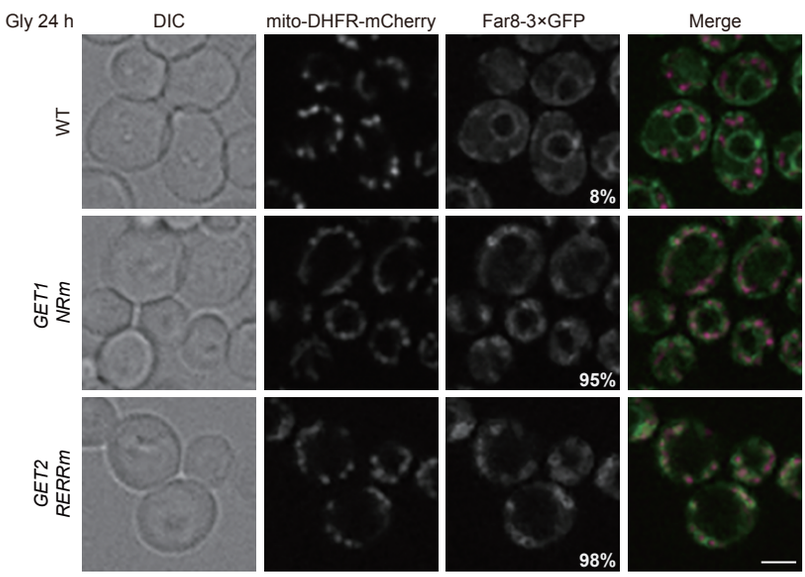

C

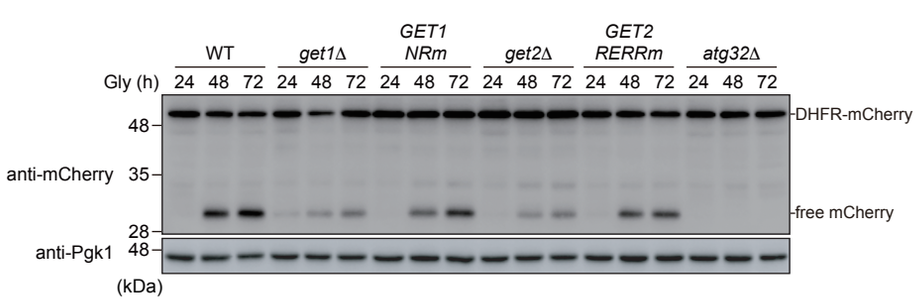

D

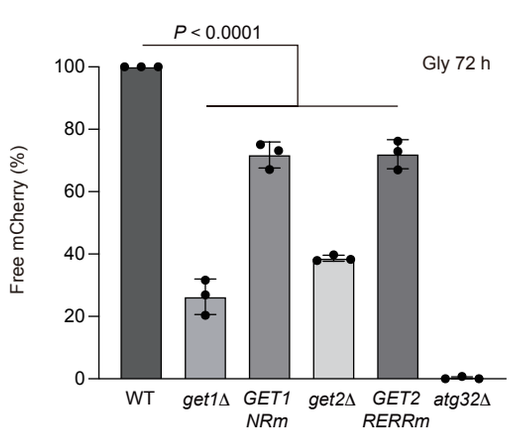

E

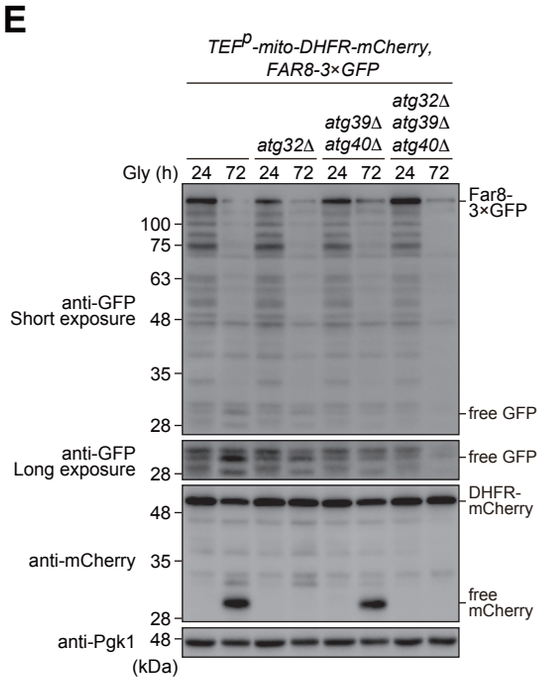

F

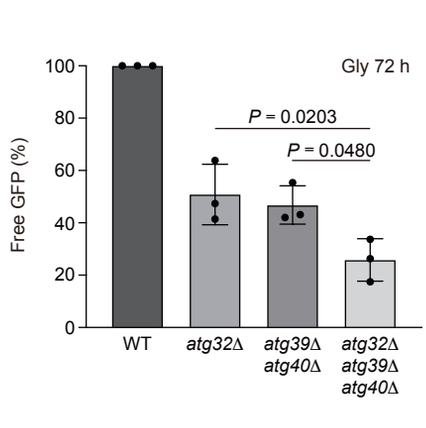

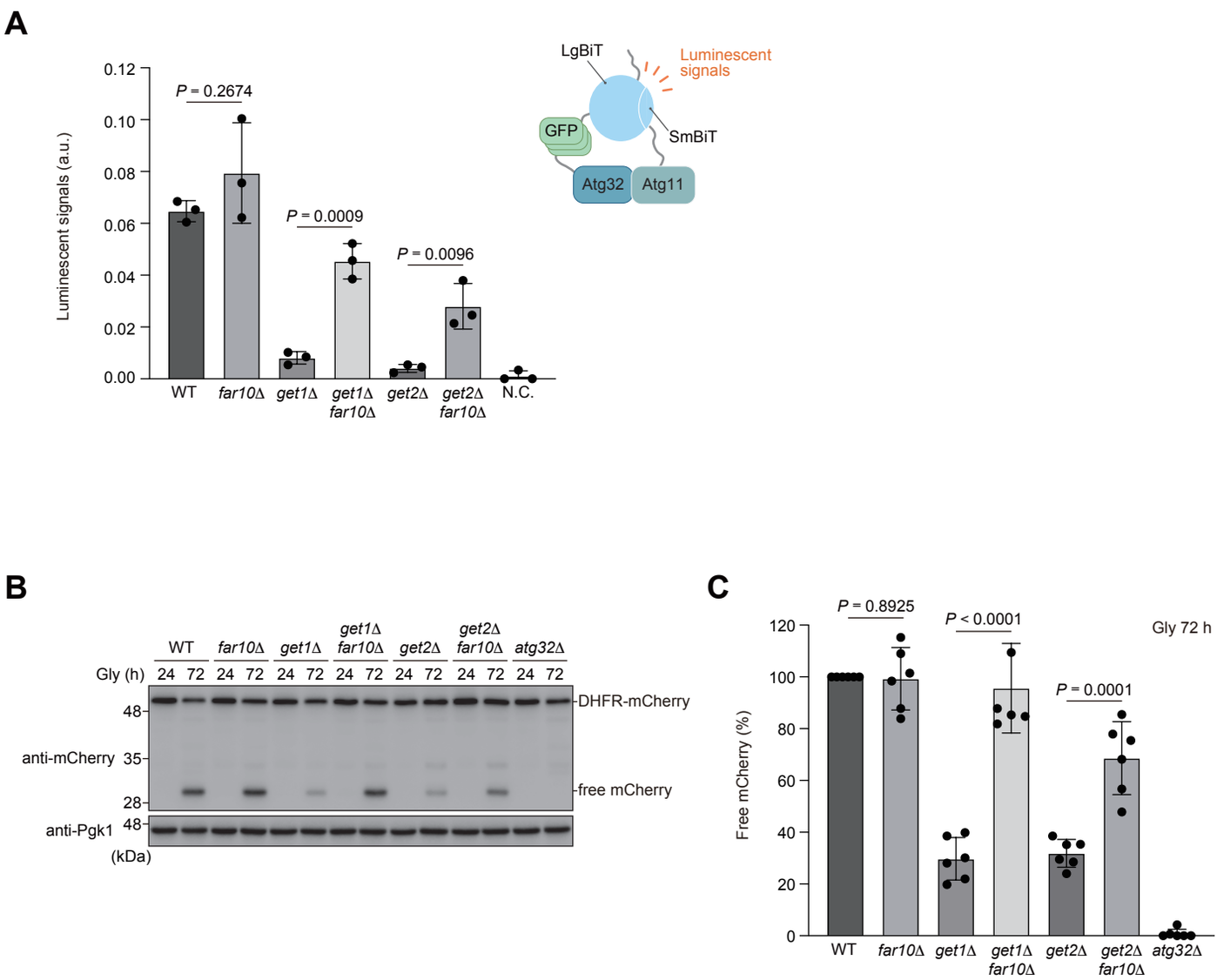

A

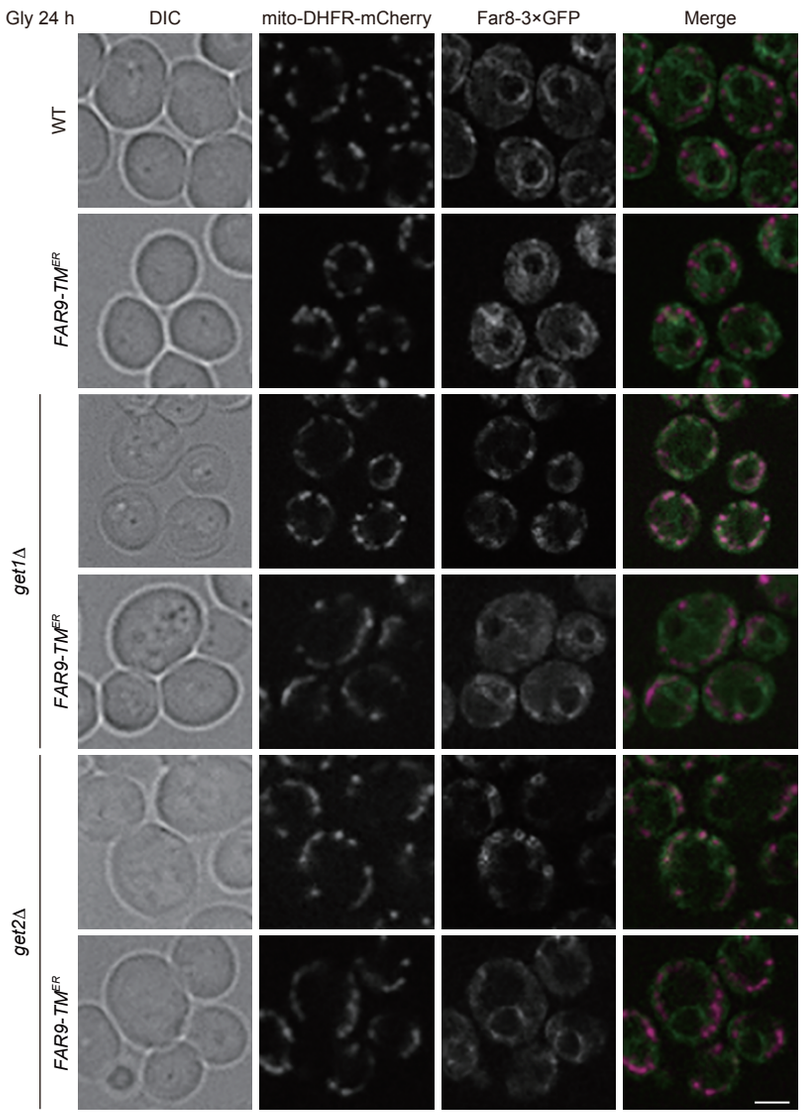

B